European Journal of Agronomy 153 (2024) 127030

Contents lists available at ScienceDirect

European Journal of Agronomy

journal homepage: www.elsevier.com/locate/eja

Can agronomic options alleviate the risk of compound drought-heat events during the wheat flowering period in southeastern Australia?

Siyi Li [a,b], Bin Wang [b,*], De Li Liu [b,c,**], Chao Chen [d], Puyu Feng [e], Mingxia Huang [f], Xiaofang Wang [g], Lijie Shi [h], Cathy Waters [i], Alfredo Huete [a], Qiang Yu [g]

[a] School of Life Sciences, Faculty of Science, University of Technology Sydney, PO Box 123, Broadway, Sydney, NSW 2007, Australia
[b] NSW Department of Primary Industries, Wagga Wagga Agricultural Institute, Wagga Wagga, NSW 2650, Australia
[c] Climate Change Research Centre, University of New South Wales, Sydney, NSW 2052, Australia
[d] CSIRO Agriculture and Food, Private Bag 5, PO Wembley, WA 6913, Australia
[e] College of Land Science and Technology, China Agricultural University, Beijing 100193, China
[f] College of Resources and Environmental Sciences, China Agricultural University, Beijing 100193, China
[g] State Key Laboratory of Soil Erosion and Dryland Farming on the Loess Plateau, Northwest A&F University, Yangling, Shaanxi 712100, China
[h] College of Hydraulic Science and Engineering, Yangzhou University, Yangzhou 225012, China
[i] NSW Department of Primary Industries, Dubbo, NSW 2830, Australia

ARTICLE INFO

Keywords:
Compound drought-heat events
Wheat flowering period
Agronomic options
Southeastern Australia
APSIM
Climate change

ABSTRACT

The impacts of compound drought-heat (DH) events on crops are more devastating than a single extreme event of drought or heat. Previous studies mainly assessed the change of individual extreme climate events. However, studies quantifying the characteristics of DH events during crop growth periods are still lacking. To the best of our knowledge, there is no study that has quantified the potential of adjusting sowing time and changing cultivars to reduce the risk of DH events for wheat in Australia. We aimed to (1) develop a combined index to capture the DH events occurring during the wheat flowering period at six study sites in southeastern Australia's wheat belt; (2) quantify the changes in the frequency (*DHF*), duration (*DHD*), and intensity (*DHI*) of DH events under future climate; and (3) identify feasible agronomic options to reduce the risk of DH events. We used the APSIM model driven by climate projections from 27 GCMs for the period of 1981–2100 to simulate the wheat flowering time and daily plant available water (PAW) at 0–100 cm soil layer. The wheat sensitive period (WSP) was defined as the period from 2 weeks before flowering to 2 weeks after flowering time. A DH event occurs when the daily maximum temperature is higher than 28 ℃ and daily PAW is less than 40% of plant available water capacity for three consecutive days or more. Then, we assessed the *DHF*, *DHD*, and *DHI* under projected climate change. Finally, we investigated the potential of changing sowing time and cultivars to alleviate *DHF*, *DHD*, and *DHI* under different climate scenarios. According to the average values across six sites, the *DHF*, *DHD*, and *DHI* during the WSP increased by 15%, 12%, and 0.9% in 2040 s, and 49%, 44%, and 5% in 2080 s, respectively, compared to 2000 s. Such increases in DH events were mainly due to enhanced heat events. Early sowing and planting better-performing wheat cultivars with early flowering had great potential to lower the risk of future DH events. They could reduce the *DHF*, *DHD*, and *DHI* by 15%– 100%, 18%– 100%, and 16%– 100%, respectively, compared to without adaptation options. However, the strategy may introduce an increased frost risk across six sites, especially in regions with climates that are less dry and hot, such as Mudgee and Wagga Wagga. We expect our modelling work can provide useful information for developing effective agronomic management practices to help Australian wheat growers better prepare for DH events under climate change. The newly proposed DH framework can be applied to other dryland wheat growing regions globally.

* Corresponding author.
** Corresponding author at: NSW Department of Primary Industries, Wagga Wagga Agricultural Institute, Wagga Wagga, NSW 2650, Australia.
E-mail addresses: bin.a.wang@dpi.nsw.gov.au (B. Wang), de.li.liu@dpi.nsw.gov.au (D.L. Liu).

https://doi.org/10.1016/j.eja.2023.127030
Received 31 January 2023; Received in revised form 8 November 2023; Accepted 8 November 2023

1. Introduction

Extreme climate and weather events are natural disasters that can plague agricultural production (Elahi et al., 2021). Instances of drought and heat disrupt the physiological processes of crops (Poudel and Poudel, 2020; Prasad et al., 2008) and reduce crop cycle duration (García et al., 2018), thus decreasing yield. For example, drought events have resulted in an estimated average reduction of 10.1% of national cereal production during 1964–2007 across the globe, with heat events contributing a similar production loss of 9.1% (Lesk et al., 2016). It's worth noting that extreme events often occur simultaneously and interact with each other (Lesk et al., 2021; Prasad et al., 2008). Often, the impacts caused by compound drought-heat (DH) events are more devastating than a single extreme event (Cohen et al., 2021; Li et al., 2022). For instance, the probability of maize yield loss was increased by 4–31% over major maize-producing countries during 1961–2016 when single heat or drought events were transformed into DH events (Feng et al., 2019b). Additionally, the European 2018 summer DH, record-high summer temperature co-occurred with record-low rainfall, led to a widespread crop harvest failure across many European countries (Bastos et al., 2020).

Wheat is the most widely planted food crop around the world (FAO, 2021), and it is the staple food source for nearly 40% of the global population (Giraldo et al., 2019). Australia is one of the top five wheat exporters in the world: Australia has contributed annually 11.3% of the global wheat exports since 1961 (FAO, 2021) and is vital for global food security. Wheat in Australia is usually grown under rain-fed conditions and often suffers from drought during the growing season (Chenu et al., 2011; Chenu et al., 2013). In addition, untimely spring heat events often occurred during wheat flowering and grain filling periods (Alexander et al., 2010; Talukder et al., 2013), aggravating the negative effects of drought on wheat. However, most previous studies focused on assessing the impact of individual extreme events such as heat or drought and adaptation strategies for the individual events, rather than on the compound extreme events that co-occur simultaneously at a specific location. Additionally, the simple addition of the effect of two single events is not enough to characterize the impacts of the compound events (Cohen et al., 2021). For example, Ababaei and Chenu (2020) assessed the impact of heat stress on wheat growth based on the modified APSIM model (Holzworth et al., 2014). Madadgar et al. (2017) used a multivariate probabilistic model to investigate yield loss probability of the five largest crops in Australia (wheat, broad beans, canola, lupine, and barley) due to drought. However, studies that quantify the characteristics and changes of DH events around wheat flowering time under climate change in Australia are still lacking.

Currently, DH events are normally investigated by combining temperature anomalies with meteorological drought indicators (monthly or seasonal precipitation, Standardized Precipitation Index, or Standardized Precipitation Evapotranspiration Index) (Geirinhas et al., 2021; Ribeiro et al., 2020; Wang et al., 2022), instead of using agricultural drought indicators. Meanwhile, due to the limitation of different temporal evolution between drought (weeks to months) and heat (days to weeks) (Mukherjee et al., 2020), most researchers defined DH events by detecting the heat events occurring within a long-term drought context (Geirinhas et al., 2021; Guo et al., 2022; Kong et al., 2020). The asymmetry of the time scale for drought (weekly, monthly, or seasonally scale) and heat (daily) in these DH frameworks leads to the inability to obtain the daily characteristics of DH events. Moreover, heat events mainly occur in the summer season, which is not the growth period of winter wheat, though several studies have investigated the DH events for summer crop maize (Feng et al., 2019b; Guo et al., 2022; Lesk et al., 2021; Li et al., 2022). Nevertheless, Australian wheat is likely to encounter simultaneous drought and heat stress around flowering time in spring, which can create nonnegligible losses in wheat grain number and grain weight (Lobell et al., 2015). To fill this knowledge gap, we developed a comprehensive combined index at a daily scale to investigate the characteristics of DH events that possibly occur during the wheat growing season.

Agronomic adaptative strategies have great potential to alleviate the impacts of extreme weather events on crops (Gouache et al., 2012; Korres et al., 2017; Vogel et al., 2019). Generally, the mechanism of these strategies includes escape and tolerance of extreme events. The escape is done through optimizing phenological development and sowing at a suitable time to avoid the susceptible growth stages of crops coinciding with the duration of abiotic stresses (e.g., frost, heat, and drought events) (Manavalan et al., 2009). For example, Stratonovitch and Semenov (2015) pointed out that a wheat cultivar with an early flowering date and longer grain filling duration had great potential to cope with heat stress compared with the existing cultivars. Additionally, Hunt et al. (2019) reported that early sowing has the potential to moderate the adverse effects of climate change on wheat in Australia. The tolerance to extreme events generally relies on the optimization of crop properties (e.g., better canopy and root architecture, stable turgor and volume of plant cells, and high strength of the antioxidant systems) (Hasanuzzaman and Fujita, 2011; Maqbool et al., 2017; Turner, 1980). For instance, Hasanuzzaman and Fujita (2011) and Mohi-Ud-Din et al. (2021) pointed out that drought and heat tolerance are dependent on the strength of the antioxidant systems of crops to endure oxidative stresses. Additionally, the traits of grain weight per tiller had a significant influence on wheat tolerance to heat and drought (Mondal et al., 2015). Compared with a single option, the combinations of early sowing and planting appropriate cultivars have a higher potential to help crops cope with extreme climate and weather events (Pirttioja et al., 2019). Semenov and Stratonovitch (2015) found that if an optimal wheat cultivar was sown 2–4 weeks earlier, the yield could be further increased by 0.2–0.6 t ha^{-1} in Europe. However, to the best of our knowledge, no study has quantified the potential for mitigating the impact of DH events on wheat in Australia through of changes in cultivars and sowing time.

In this study, we used the APSIM-wheat model to simulate wheat phenology and soil water content. The DH events occurring in the wheat flowering period were firstly defined. Then, we evaluated characteristics of DH events under the historical and future climates based on 27 different global climate models (GCMs) from the Coupled Model Intercomparison Project Phase 6 (CMIP6) under two emission scenarios at six study sites in southeastern Australia. Also, we assessed the potential of sowing earlier and adopting different wheat cultivars to reduce the risk of DH events. The main objectives of this study were to (1) develop a combined index to capture the DH events occurring during the wheat flowering period at six study sites in southeastern Australia's wheat belt; (2) quantify the changes in the DH frequency (*DHF*), DH duration (*DHD*), and DH intensity (*DHI*) under future climate; and (3) identify feasible agronomic options to reduce the risk of future DH events.

2. Materials and methods

2.1. Study sites

The New South Wales (NSW) wheat belt is located in the southeast of Australia and spans a wide range of topographical and climatic conditions. The eastern parts consist of mountains up to 1100 m in elevation, while the western parts are mainly plains (Feng et al., 2020). During the wheat growing season (typically April-November), the rainfall gradient is increased from 172 mm in the west to 763 mm in the southeast. Conversely, the average temperature in the growth period gradually rises from southeast to northwest, ranging from 8.3 ℃ to 17.1 ℃ (Wang et al., 2017a). We selected six sites representing different agro-climatic zones across the NSW wheat belt in this study (Table 1). They are Walgett and Moree plains in the north of the wheat belt, Lachlan and Mudgee in the middle, and Balranald and Wagga Wagga located in the south (Fig. 1). Wheat is grown under rain-fed conditions in the NSW wheat-belt, where it is sown in autumn (April-July), flowers in early to mid-spring, and matures in late spring (Liu, 2007; Wang et al., 2015a).

Table 1
Total rainfall, average value of daily maximum temperature (T_{max}), average value of daily minimum temperature (T_{min}), average value of daily mean temperature (T_{mean}), and plant available water holding capacity (PAWC) (0–100 cm) in the wheat growing season (April - November) from 1981 to 2020 at the six study sites (Walgett, Moree Plains, Lachlan, Mudgee, Balranald, and Wagga Wagga).

Sites	Latitude	Longitude	Rainfall (mm)	T_{max} (℃)	T_{min} (℃)	T_{mean} (℃)	PAWC (mm)
Walgett	-29.66	148.12	255.4	24.4	9.7	17.0	117.5
Moree Plains	-29.50	149.90	319.7	23.5	9.4	16.5	165.4
Lachlan	-33.10	146.85	277.3	21.1	7.7	14.4	129.1
Mudge	-32.60	149.60	438. 9	19.6	5.7	12.6	89.7
Balranald	-34.20	143.50	194. 5	21.2	7.7	14.4	92.0
Wagga Wagga	-35.05	147.35	365.1	18. 8	6.4	12.6	92.0

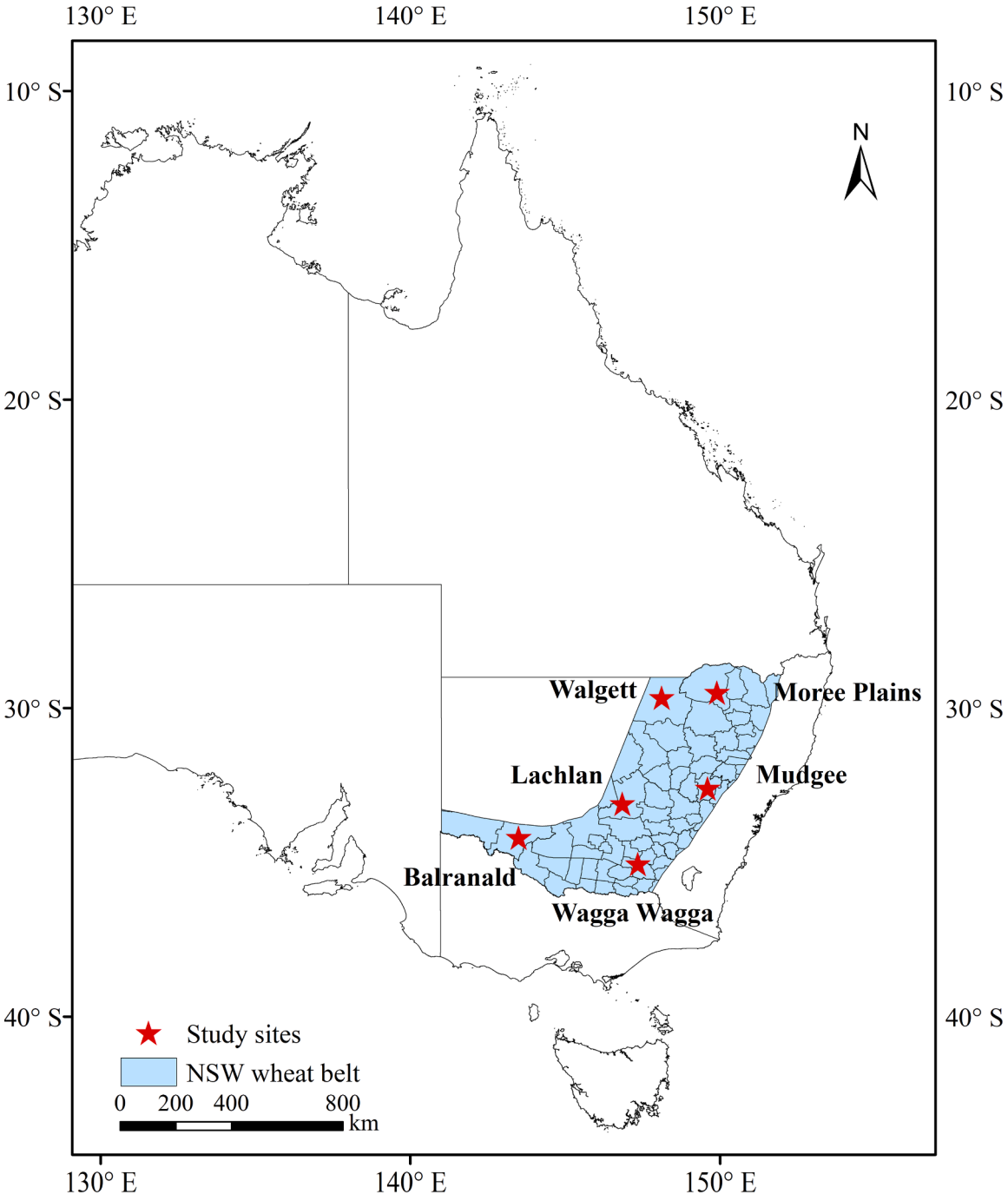

Fig. 1. The location of six selected sites in New South Wales (NSW) wheat belt in southeastern Australia.

2.2. Data sources

2.2.1. Climate data

We downloaded the monthly gridded climate data for 27 GCMs of CMIP6 (Table S1) from 1900 to 2100 from World Climate Research Program (WCRP) (https://esgf-node.llnl.gov/search/cmip6/). The simulation of CMIP6 was conducted under the combination of a representative concentration pathway (RCP) and a shared socio-economic pathway (SSP). We selected the data under SSP245 and SSP585 scenarios. SSP245 represents the scenario combining a middle socio-economic development road (SSP2) with the medium-low radiative forcing of 4.5 W/m^2 (RCP4.5). SSP585 represents the scenario combining a high energy-intensive, socio-economic developmental path (SSP5) with high radiative forcing 8.5 W/m^2 (RCP8.5) (Grose et al., 2020; Li et al., 2020; Yang et al., 2021; You et al., 2021).

Normally, the future climate projections from GCMs have coarse spatiotemporal resolution and cannot be directly used at study sites. We used a statistical downscaling method, NWAI-WG, proposed by Liu and Zuo (2012) to downscale the daily climate data for six selected sites. The specific procedures were as follows: firstly, the raw GCM data were downscaled to specific climate sites of interest by an inverse distance-weighted interpolation method. Then, we corrected the bias of monthly GCMs values for each site, making it consistent with the observed values. According to the correlation between historical climate data and future climate predictions, we calculated the parameters of the Stochastic Weather Generator (WGEN) (Richardson and Wright, 1984). Finally, the monthly scale value after bias correction was downscaled to the daily value through the modified WGEN.

2.2.2. Soil data

We obtained the soil hydraulic properties and other soil parameters from the Australian Soil Resource Information System (http://www.asris.csiro.au/). There were more than 800 soil profiles in agricultural areas of Australia, and most of them were parameterized for modeling (Dalgliesh et al., 2012). We used the soil profiles that are geographically closest to the six sites (Feng et al., 2020; Innes et al., 2015). Plant available water capacity (PAWC) represents the total amount of water a soil can store for crop to use. PAWC is calculated as the difference of volumetric water content between the upper drainage limit (DUL) and crop lower limit (Asseng et al., 2001; Wang et al., 2017b). The value of LL is specific to the crop, we used wheat LL in this study. The range of soil PAWC (0–100 cm) for six sites is from 89.7 to 165.4 mm (Table 1), due to different soil types in different regions.

2.3. APSIM model

We used APSIM (Agricultural Production Systems sIMulator) version 7.10 to simulate the phenology of wheat and soil water content on a daily basis for baseline period (2000 s: 1981–2020) and two future periods (2040 s: 2021–2060, 2080 s: 2061–2100). APSIM is an agricultural production system simulation model developed by the Agricultural Production Systems Research Group (APSRU) in collaboration between CSIRO and Queensland Government (Holzworth et al., 2014; Keating et al., 2003). The model system has been widely validated and used all over the world and has played a powerful role in agricultural research (Amarasingha et al., 2015; Archontoulis et al., 2014; Flohr et al., 2018; Seyoum et al., 2017; Wang et al., 2017b). In particular, the APSIM wheat module has been applied in many studies throughout Australian agricultural areas (Asseng et al., 2011; Chenu et al., 2013). It can adequately simulate the growth process of wheat (Anwar et al., 2015) and the dynamics of soil water and nitrogen in agricultural systems (Archontoulis et al., 2014; Liu et al., 2014). Also, APSIM can assess the potential of different agronomic options (e.g., adjusting sowing date and changing different cultivars) to cope with climate change (Wang et al., 2019; Xiao et al., 2020).

Our simulations mainly involved wheat phenology and soil water dynamics. In the APSIM-Wheat model, wheat is divided into eight phases from sowing to maturity: 1) sowing to germination, 2) germination to emergence, 3) emergence to end of juvenile stage, 4) end of juvenile stage to floral initiation, 5) floral initiation to flowering, 6) flowering to start of grain filling, 7) start of grain filling to end of grain filling, and 8) end of grain filling to physiological maturity. The length of each phase is determined by the required accumulation of thermal time, which is modified by additional factors specific to each phase, such as vernalization and photoperiod (APSIM, 2015).

The SoilWat module is used to simulate the soil moisture status. It is a cascading water balance model that evolved from CERES (Jones and Kiniry, 1986) and PERFECT (Littleboy et al., 1992). SoilWat can simulate hydrological processes, including runoff, evaporation, saturated water flow, unsaturated water flow, leaching, and above saturation flow between layers on a daily basis, based on the lower limit (LL15), DUL, saturated (SAT), crop lower limit (CLL), and other hydraulic parameters. More detailed information about APSIM can be found in previous studies (Asseng et al., 2000; Hao et al., 2021; Keating et al., 2003).

2.4. APSIM simulations

We ran simulations for 6 sites with 27 GCMs over 1981–2100 under two emission scenarios using the APSIM-wheat model. The wheat cultivar *Janz* was used in this study. Due to its prevalence in NSW, this mid-maturity spring cultivar is widely cultivated and serves as a suitable representative for studying the impacts of climate change on wheat in the region (Kirkegaard and Lilley, 2007; Wang et al., 2009). In addition, *Janz* has also been well-parameterized in the APSIM model (Zheng et al., 2012). Based on the target sowing window between 27th April to 15th July (day 117 to day 196) for wheat *Janz* proposed by Zheng et al. (2012), we set a sowing rule to mimic real farm sowing practices. This approach considered the present soil water and the current rainfall to meet the certain moisture condition or when the sowing window is coming to an end. Sowing occurred when the following rule was met:

$$R_k \geq PAWC_{50} \times CR_k - SW_{k-1} \tag{1}$$

$$CR_k = \sqrt[3]{\frac{CA}{(1 + CB \times D_k)}} \tag{2}$$

$$CB = \frac{{A_2}^3 - {A_1}^3}{S_s \times {A_1}^3 - S_e \times {A_2}^3} \tag{3}$$

$$CA = {A_1}^3 + S_s \times {A_1}^3 \times CB \tag{4}$$

where R_k is rainfall of the kth day in the sowing window (27th April to 15th July); $PAWC_{50}$ is the plant available water capacity within 50 cm; $SW_{k\text{-}1}$ is the previous day's soil water content within the sowing window; CR_k is the inverse proportional function of the D_k (Eq. (2)); D_k is day of year for the kth day in the sowing window. According to the sowing window we set, the value of CR_k was between 1.2 and 0.8, which gradually decreased with time. This setting balanced the limits of the sowing window and the need for soil moisture condition. We showed the CR_k value in 1981 of site Walgett as an example for better description (Fig. S1). $A_1 = 1.2$; $A_2 = 0.8$; S_s and S_e are the day of year for the start and the end of the sowing window, respectively. We set the sowing window from $S_s = 117$ to $S_e = 196$.

Due to the spatial heterogeneity of the soil profile and the spatiotemporal variations of precipitation, the soil water content is dynamic and varies in different sites. Our sowing rule aimed to make wheat in different regions across the wheat-belt sown under the most favorable water conditions in the sowing window, thus ensuring a higher germination rate. We considered that this is more reasonable and realistic than a sowing rule based on the amount of recent rainfall for sites across different rainfall zones with different soil moisture content during the sowing season. According to the sowing rules, soil properties, and

climate projections of 27 GCMs, we performed the first set of APSIM simulations to identify the wheat phenology and plant available soil water (PAW). The output wheat phenological data and daily PAW data were used to determine and calculate the frequency, duration, and intensity of DH events in the sensitive flowering period of wheat. We analyzed their temporal and spatial variations, and they were used as the control scenarios without agronomic adaptative options to verify the potential of the agronomic options in avoiding DH events.

2.5. Drought, heat, and compound drought-heat events in the wheat flowering period

The wheat flowering period is critical to wheat growth and development (Cossani et al., 2009). It determines the wheat grain number and grain weight (Dias and Lidon, 2009; Frank and Bauer, 1982; Rawson and Bagga, 1979), and also is highly susceptible to heat and drought stress (Saini and Westgate, 1999; Shah and Paulsen, 2003; Stratonovitch and Semenov, 2015; Talukder et al., 2014; Vignjevic et al., 2015). Specifically, extreme events that occurred during the period from pre-flowering to 3 days after flowering can result in grain sterility and abortion (Tashiro and Wardlaw, 1990), which in turn reduces grain number. The extreme events that occurred 6–14 days after flowering led to a decline in the storage capacity of cereal grains (Saini and Westgate, 1999; Tashiro and Wardlaw, 1990), thereby diminishing the grain size and single-grain weight. We selected the period from 2 weeks before flowering to 2 weeks after flowering as the wheat sensitive period (WSP, 29 days) in this study. The WSP includes the heading stage, the flowering stage, part of the critical period for grain set, and the start of the linear phase of grain filling of wheat (APSIM, 2015; Pimstein et al., 2009; Zadoks et al., 1974). The annual WSPs at six sites were obtained based on the wheat flowering time simulated by APSIM.

We selected the general and well-accepted criteria to define drought and heat events in the WSP. That is, using the threshold of PAW to define whether wheat suffered water stress, and the threshold of daily maximum temperature (*TX*) was used to define whether heat stress occurred. Many experimental studies have found that 40% of PAWC can be the threshold for distinguishing water stress on wheat (Ciais et al., 2005; Granier et al., 1999). When the PAW falls below 40% of PAWC, the water uptake of wheat can be restricted, leading to adverse impacts on wheat growth and development, ultimately influencing the formation of yields (Kirkegaard and Lilley, 2007; Wenda-Piesik, 2011). Therefore, a drought event was triggered when PAW in the 0–100 cm soil profile was lower than 40% of PAWC in this profile for consecutive three or more days. The reason why we only considered PAW in 0–100 cm soil layer is that the majority of wheat roots are distributed in 0–30 cm with a small fraction below 30 cm (Chen et al., 2014) and further with few roots below 100 cm (Fan et al., 2016; Gan et al., 2011). Considering a very small fraction of roots below 100 cm which has a small contribution to total water uptake, in this study we focused on the PAWC and soil water content within the 0–100 cm soil layer. In terms of heat definition, the optimal temperature range is normally 18 °C − 28 °C around the wheat flowering stage (Mullarkey and Jones, 2000; Porter and Gawith, 1999). We used 28 °C as a threshold of temperature tolerance during the flowering period. When the daily maximum temperature is higher than 25–28 °C, the size and weight of wheat grain will be smaller (Lalic et al., 2013; Wheeler et al., 1996). Therefore, we defined heat events during WSP when the daily *TX* is higher than 28 °C for three consecutive days or more (Dodd et al., 2021; Mukherjee and Mishra, 2021; Mullarkey and Jones, 2000; Ristic et al., 2007). Based on the above-mentioned criteria for the definition of drought and heat events during WSP, we defined a compound DH event when heat and drought events occur simultaneously. Table 2 shows an example of one DH event occurring during the WSP.

We characterized the DH events from three dimensions: frequency, duration, and intensity. *DHF* refers to the ratio of the accumulative sum days of all DH events in WSP to the length of the window (29 days); *DHD* represents the maximum number of days within DH events in the WSP; *DHI* was defined as the mean weighted sum of PAW and *TX* excesses over the drought and heat thresholds, respectively, over the WSP.

$$DH_j = d_i \left| \left\{ \left(TX_{ij} \geq T_c\right) \cap \left(PAW_{ij} £ \delta \leq PAWC\right) \right\}, j = 1, 2, ., N; i = l+1, l+2, ., l+m_j, m_j \geq 3; w_s \leq d_i \leq w_e \quad (5)$$

where DH_j is the jth DH event; N is the number of DH events in each WSP; d_i is the ith day in the WSP with the subscript l presenting the day before the start of the jth DH event; TX_{ij} is the maximum temperature of d_i in the jth DH event; T_c is the heat threshold temperature, which we took as 28 ℃; PAW_{ij} is plant available water at d_i in the jth DH event; $\delta$is a constant to set starting point for drought effect as the amount of PAW ($\leq \delta \times PAWC$) in WSP, we set $\delta = 0.4$(Ciais et al., 2005; Granier et al., 1999); w_s is the start day of WSP; w_e is the end day of WSP.

DHF was calculated as the cumulative sum of the consecutive days during each DH event (Eq. (6)) in the WSP dividing by the length of the WSP (29 days).

$$DHF = \frac{\sum_{j=1}^{N} m_j}{w_e - w_s + 1}, j = 1, 2, ., N, N \geq 1 \quad (6)$$

Table 2
Example of one compound drought-heat (DH) event occurring during the wheat sensitive period (WSP). d_i is the ith day in the WSP; w_s is the start day of WSP; w_e is the end day of WSP; TX_i is the maximum air temperature of ith day in WSP; PAW_i is the plant available water of ith day in WSP; $PAWC$ is plant available water capacity in 0–100 cm soil layer; DH_j is the jth DH event in the WSP.

d_i	$TX_i \geq 28$ ℃	$PAW_i \leq \delta \times PAWC$	
w_s	TRUE	FALSE	
…	FALSE	TRUE	
l+1	TRUE	TRUE	DH_j
l+2	TRUE	TRUE	
…	TRUE	TRUE	
l+m_j	TRUE	TRUE	
…	FALSE	FALSE	
w_e	TRUE	TRUE	

DHI was calculated based on the mean value of the daily intensity during the consecutive days of DH event over the WSP. We obtained the daily intensity by weighting the sum of the daily standardized values of drought intensity and the intensity of heat. The drought intensity is represented by the difference between the drought threshold ($\delta \times PAWC$) and the daily PAW divided by the difference between the drought threshold and the plant available water threshold of wheat permanent wilting point. It is a dimensionless value between 0 and 1, 1 is the highest drought intensity (Eq. (7)).

$$DI_{ij} = \frac{\delta \times PAWC - PAW_{ij}}{\delta \times PAWC}, i = 1, 2, ., m_j; j = 1, 2, ., N \quad (7)$$

where DI_{ij} is the daily drought intensity for the ith day of the jth DH event in a given year; $\delta \times PAWC$ is the threshold to define drought according to extractable water, in which $PAWC$ is defined by soil properties; PAW_{ij} is the plant available water on the ith day of the jth DH event.

Heat intensity was defined by Eq. (8). The ratio of TX exceeding the heat threshold (T_c) to the wheat high killing temperature (T_s) exceeding of T_c was calculated as the heat intensity. Also, it is a dimensionless value between 0 and 1. 1 is the highest heat intensity.

$$HI_{ij} = \frac{TX_{ij} - T_c}{T_s - T_c}, i = 1, 2, ., m_j; j = 1, 2, ., N \quad (8)$$

where HI_{ij} is the daily heat intensity for the ith day of the jth DH event in a given year; TX_{ij} is the maximum temperature for the ith day of the jth DH event. We took T_s (the wheat high killing temperature) as 42 ℃, because Kumar Tewari and Charan Tripathy (1998) pointed out that wheat was killed when exposed to 42 ℃ for more than 48 h.

The daily *DHI* was calculated as the sum of the daily standardized values of heat intensity and drought intensity.

$$SDH_{ij} = \alpha DI_{ij} + (1 - \alpha) HI_{ij}, i = 1, 2, ., m_j; j = 1, 2, ., N \quad (9)$$

$$CDH_j = \frac{\sum_{i=1}^{m_j} SDH_{ij}}{m_j}, j = 1, 2, ., N \quad (10)$$

$$DHI = \frac{\sum_{j=1}^{N} CDH_j}{N}, j = 1, 2, ., N, N \geq 1 \quad (11)$$

where SDH_{ij} is the daily DH intensity for the ith day of the jth DH event in a given year; α is the weight for daily drought intensity, we used 0.5; CDH_j is the DH intensity for the jth DH event in the given year.

2.6. Agronomic adaptation options

Our study used two adaptation options: changing cultivars and sowing on an earlier date. *Janz* was used as a reference cultivar for designing virtual wheat genotypes. It is a mid-mature cultivar and does not require strong vernalization. When designing virtual wheat cultivars, we only modified three genetic parameters (tt_end_of_juvenile (TTEJ), tt_floral_initiation (TTFI), and tt_flowering (TTFW)) which affect phenology, to control the timing of wheat flowering and make the WSP escape from DH events, generating $4^3 = 64$ virtual wheat varieties. Detailed definitions of these parameters can be found in Table 3. Early sowing is widely considered to be helpful for Australian wheat to cope with climate change. Therefore, we advanced the original sowing window by one and two weeks, respectively, that is, day 110 to day 189 (20 April to 8 July) and 103–182 (13 April to 1 July). After advancing the sowing window, specific early sowing dates were still determined according to the sowing rules in 2.4. Based on the settings of these adaptive options, we ran a second set of APSIM simulations using 27 GCMs data to test the potential of individuals and combined the two adaptations in reducing DH risk in WSP, respectively. Then, we selected the agronomic options corresponding to minimum *DHF*, *DHD*, and *DHI* under the 2040 s and 2080 s at the six sites, respectively, as the better-performing agronomic options.

2.7. Data visualization

We conducted APSIM simulations based on 27 climate change models (GCMs) under two emission scenarios (SSP245 and SSP585), covering the period from 1981 to 2100. This resulted in 27 annual estimations of different DH indices for each year within each scenario. Initially, we calculated the multi-year average of each DH indices for the 2000 s (1981–2020), 2040 s (2021–2060), and 2080 s (2061–2100) using the annual data, as we present our data according to these three periods in all figures. Then to synthesize these multiyear average estimations from the 27 GCMs into a single representation, we employed ensemble averaging. The single representations for the 2000 s, 2040 s, and 2080 s under two scenarios at the six study sites were displayed in bar plots.

To create the box plot for projected changes in DH indices after adopting each adaptation, we initially computed the multiyear average of DH indices for the 2040 s and 2080 s using annual data from 27 GCMs, both before and after adaptation. Subsequently, we then compared the difference in DH indices between before and after adaptation, within each GCM and time period. The projected changes in DH indices in the 2040 s and 2080 s from the 27 GCMs were directly visualized in the boxplot. Box boundaries indicate the 25th and 75th percentiles across GCMs, and whiskers below and above the box indicate the 10th and 90th percentiles. The black lines and crosshairs within each box indicate the multi-model median and mean respectively.

3. Results

3.1. Projected change in wheat flowering window

Fig. 2 shows the projected changes in wheat flowering time between two future periods (2021–2060 and 2061–2100) and the baseline period (1981–2020) at six sites. The wheat flowering time was projected to be advanced in the future at all sites, with more advanced under SSP585 than under SSP245. Specifically, the wheat flowering time was 5–17

Table 3
The reference cultivar (*Janz*) and range of three genetic parameters selected in the APSIM model. The $3 * 4^3 = 192$ agronomic options were generated by all possible combinations of different parameters and sowing window.

Sowing window	Cultivar parameters	Definition	Unit	Step	*Janz*	Minimum value	Maximum value
27 April to 15 July	TTEJ	Thermal time from emergence to end of juvenile	°C·day	100	400	300	600
	TTFI	Thermal time from end juvenile to floral initiation	°C·day	100	458	358	658
	TTFW	Thermal time from floral initiation to flowering	°C·day	30	109	79	169
20 April to 8 July	TTEJ	Thermal time from emergence to end of juvenile	°C·day	100	400	300	600
	TTFI	Thermal time from end juvenile to floral initiation	°C·day	100	458	358	658
	TTFW	Thermal time from floral initiation to flowering	°C·day	30	109	79	169
13 April to 1 July	TTEJ	Thermal time from emergence to end of juvenile	°C·day	100	400	300	600
	TTFI	Thermal time from end juvenile to floral initiation	°C·day	100	458	358	658
	TTFW	Thermal time from floral initiation to flowering	°C·day	30	109	79	169

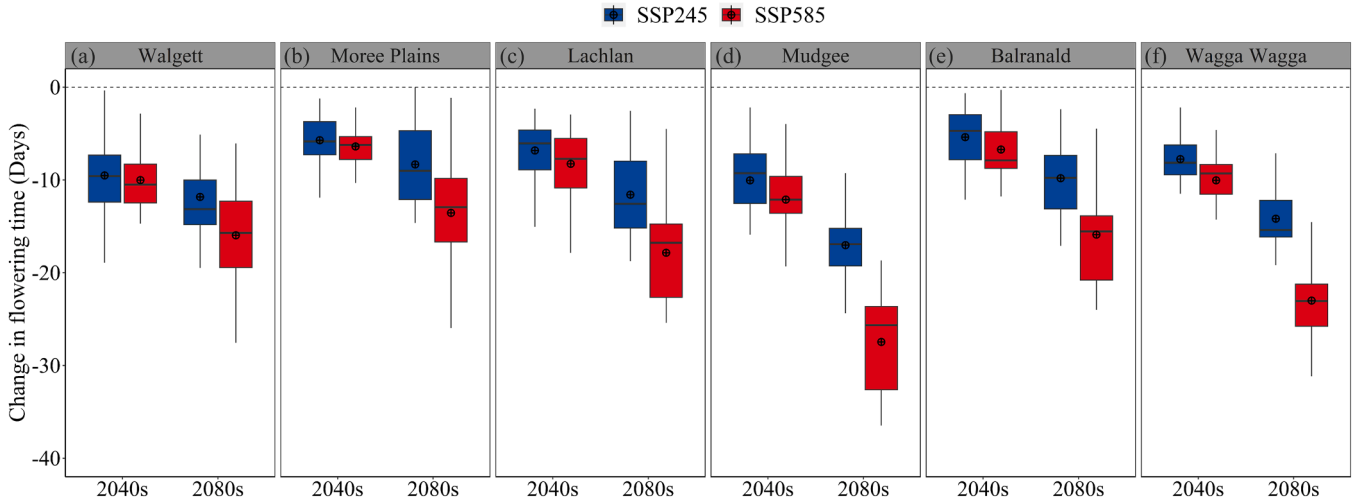

Fig. 2. Projected changes in simulated flowering time at six sites. Changes were estimated between two future periods (2021–2060 and 2061–2100) and the baseline period (1981–2020) under SSP245 and SSP585 based on the 27 downscaled GCMs. Box boundaries indicate the 25th and 75th percentiles across GCMs, whiskers below and above the box indicate the 10th and 90th percentiles. The black lines and crosshairs within each box indicate the multi-model median and mean, respectively.

days earlier in the 2040 s and 2080 s under SSP245 compared to the 2000 s. Under SSP585, wheat flowering time was 6–27 days earlier than that of the 2000 s. Across the six sites, the flowering time of wheat in sites Mudgee and Wagga Wagga, which are located in the southeastern NSW wheat belt, was obviously earlier than that of the other four sites.

3.2. The characteristics and changes of DH

Fig. 3 shows the *DHF*, *DHD*, and *DHI* in WSP at six sites under SSP245 and SSP585 using 27 GCMs in the 2000 s, 2040 s and 2080 s. According to the six-site average values, the *DHF*, *DHD*, and *DHI* in WSP increased by 15%, 12%, and 0.9% in 2040 s, and 49%, 44% and 5% in 2080 s, respectively, compared with 2000 s. The *DHF* in northern wheat belt, i.e., Walgett and Moree Plains were higher than that at other four sites (Fig. 3a-b). In 2000 s, 2040 s, and 2080 s, the *DHF* at Walgett and Moree Plains were 0.01–0.14, 0.10–0.28, and 0.11–0.35 higher than that of the other four sites under SSP245, respectively. Also, similar changes appeared under SSP585. In the future, the *DHF* would increase at all sites except Balranald (Fig. 3e). Walgett had the largest *DHF* increases by 0.19 and 0.24 in 2040 s and 2080 s under SSP245, and 0.21 and 0.30 under SSP585, respectively (Fig. 3a). Moreover, when comparing sites with similar latitude, the western sites had slightly higher *DHF* than that of the eastern sites. According to the average value of 2000 s, 2040 s, and 2080 s under SSP245, the *DHF* at Walgett was 0.07 higher than that at

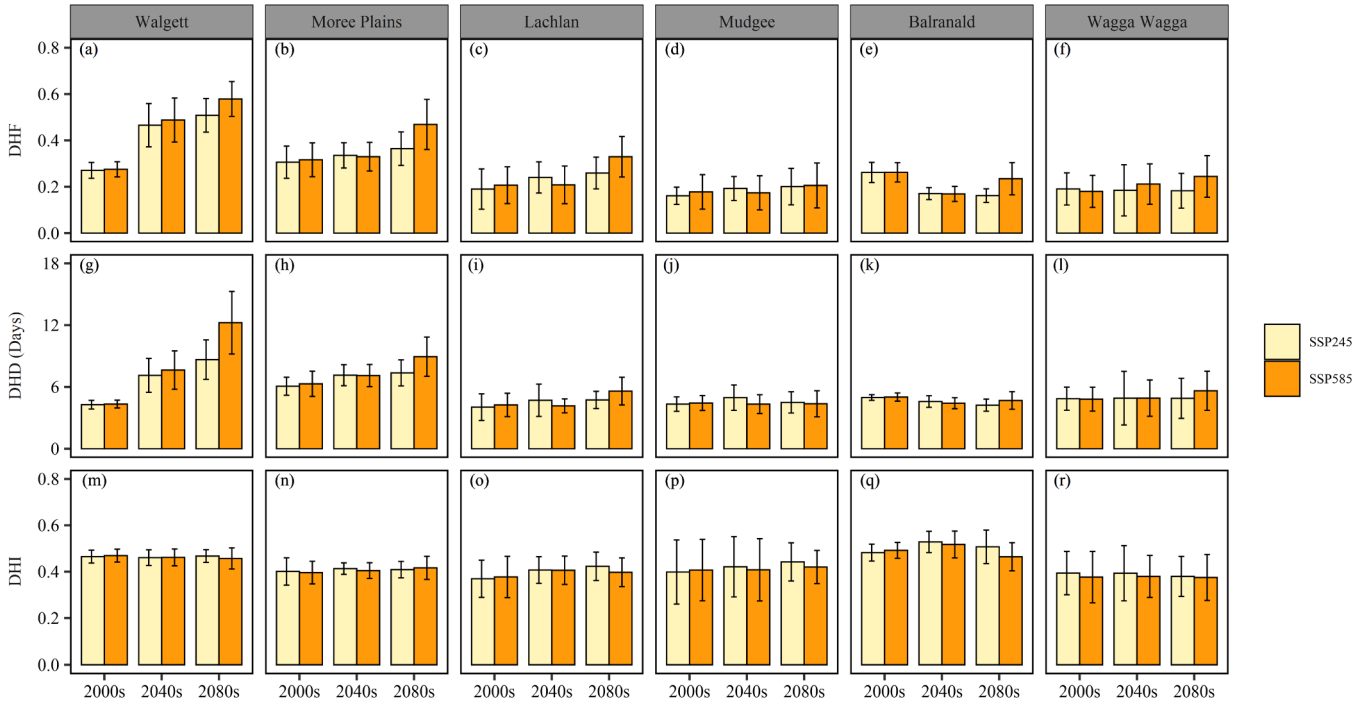

Fig. 3. The averaged frequency (*DHF*), duration (*DHD*), and intensity (*DHI*) of compound drought-heat events during the wheat sensitive period (WSP) at six sites under SSP245 and SSP585 based on 27 GCMs in the 2000 s (1981–2020), 2040 s (2021–2060), and 2080 s (2061–2100). The error bar represents the standard deviation of 27 GCMs.

Moree Plains, *DHF* at Lachlan was 0.05 higher than that at Mudgee, and the *DHF* at Balranald was 0.01 higher than that at Wagga Wagga. Similar to *DHF*, the *DHD*s at Walgett and Moree Plains were the highest among all six sites (Fig. 3g-h), and their higher *DHD* was extended into the future. *DHD* would increase most in Walgett (Fig. 3g), which was extended 3 days under both two SSPs in 2040 s *DHD* in 2080 increased more obviously, which were 4 and 8 days under SSP245 and SSP585, respectively. Also, the *DHD* at Lachlan was slightly increased in the future (Fig. 3i), while there was little difference between their historical and future *DHD* at Mudgee, Balranald, and Wagga Wagga (Fig. 3j-l). In addition, the changes in *DHI* at six sites were not significant in the future. There would be a slight increase in future *DHI* at Moree Plains, Lachlan, Mudgee, and Baranald (Fig. 3h-k), while the future *DHI* was almost the same as the historical *DHI* at Walgett and Wagga Wagga (Fig. 3g&l). Balranald, the lowest rainfall site presented a high drought intensity and thus had the highest *DHI* among all six sites (Fig. 3q). The characteristics and changes of individual drought and heat events can be found in the supplementary materials (section S1).

3.3. Effects of changing wheat cultivars and sowing earlier

After comparing the DH indices of 64 virtual wheat cultivars at six sites in 2040 s and 2080 s, we selected the cultivars corresponding to the minimum *DHF*, *DHD*, and *DHI* as the better-performing wheat cultivars for each period at each site. Fig. 4 represents the reduction rates of *DHF*, *DHD*, and *DHI* after planting better-performing wheat cultivars compared with those when planting *Janz*. The six-site average *DHF*, *DHD*, and *DHI* decreased by 44%, 41%, and 42%, respectively, after sowing the better-performing wheat cultivars at all sites, throughout 2040–2080 s under SSP245. For the two future periods, there were better effects on alleviating DH risk in 2040 s compared to that in 2080 s *DHF* values averaged across 6 sites would be decreased by 51% and 48% under SSP245 and SSP585 in 2040 s, but in 2080 s only by 37% and 21%, respectively. Similar changes were observed in the other two indices. That is, according to average values of six sites under SSP245, the *DHD* and *DHI* were decreased by 47% for both indices in 2040 s and by 36% and 38% in 2080 s, respectively. Under SSP585, *DHD* and *DHI* decreased by 45% and 48% in 2040 s, and by 22% and 27% in 2080 s, respectively. Comparing the results among six sites, we found that the reduction rates of DH indices in the three eastern sites (Moree Plains, Mudgee, and Wagga Wagga) of the wheat belt were higher than those in the western sites (Walgett, Lachlan, and Balranald) at similar latitudes. For instance, the reduction percentage of *DHI* under SSP245 was 10%, 25%– 53%, and 23%– 45% higher at Moree Plains, Mudgee, and Wagga Wagga (Fig. 3n, p, and r) than Walgett, Lachlan, and Balranald (Fig. 3m, o, and q), respectively, across 2040 s and 2080 s. Also, similar changes were presented in *DHF* and *DHD* under two SSPs, except for the reduction rates of *DHF* at Moree Plains (Fig. 4b) were lower than that in Walgett (Fig. 4a).

We compared the changes in *DHF*, *DHD*, and *DHI* of different sowing window at six sites in 2040 s and 2080 s under SSP245 and SSP585, then selected the sowing window corresponding to the minimum *DHF*, *DHD*, and *DHI* as the ideal sowing time. The *DHF*, *DHD*, and *DHI* in the WSP at six sites were decreased under SSP245 and SSP585 after applying ideal sowing time (Fig. 5). The six-site average reduction rates in *DHF*, *DHD*, and *DHI* were 28%, 28%, and 16%, respectively, throughout 2040–2080 s under SSP245. However, the alleviation effects of ideal sowing time on DH in 2040 s were better than that in 2080 s. According to the average values of six sites, the *DHF* were reduced by 34% in 2040 s, but only by 22% in 2080 s after applying ideal sowing time under SSP245. In addition, the ideal sowing time had better effects on alleviating DH in three southeastern sites (Mudgee, Balranald, and Wagga Wagga) (Fig. 5d-f, j-l, and p-r) than three northwestern sites (Walgett, Moree Plains, and Lachlan) (Fig. 5a-c, g-i, and m-o). For example, under SSP245, *DHD* reducing rates in three southeastern sites were from 21% to 65% throughout 2040 s and 2080 s, higher than

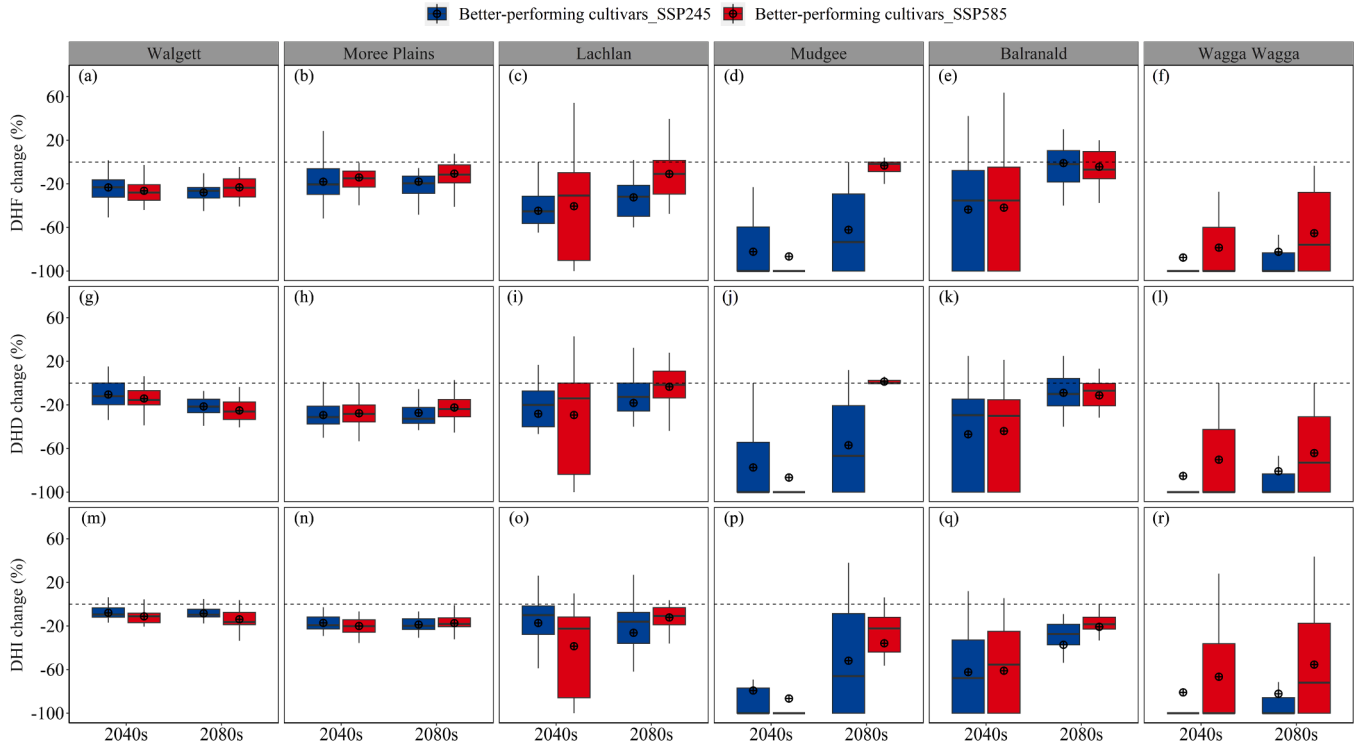

Fig. 4. Projected changes in compound drought-heat frequency (*DHF*), duration (*DHD*), and intensity (*DHI*) during the wheat sensitive period (WSP) at six sites. Changes were estimated between before and after adopting better-performing wheat cultivars for 2040 s (2021–2060) and 2080 s (2061–2100) under SSP245 and SSP585 based on the 27 GCMs. Box boundaries indicate the 25th and 75th percentiles across GCMs, whiskers below and above the box indicate the 10th and 90th percentiles. The black lines and crosshairs within each box indicate the multi-model median and mean, respectively.

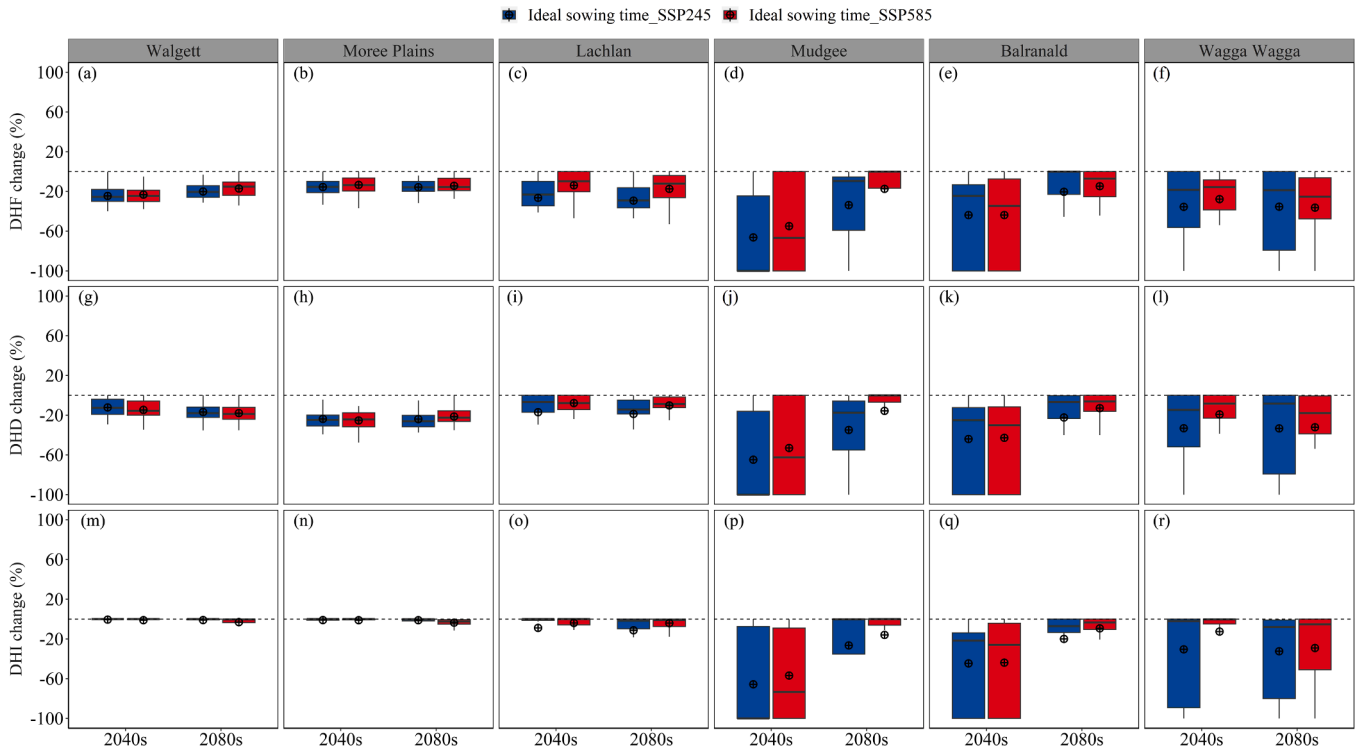

Fig. 5. Projected changes in compound drought-heat frequency (*DHF*), duration (*DHD*), and intensity (*DHI*) during the wheat sensitive period (WSP) at six sites. Changes were estimated between before and after using ideal sowing time for 2040 s (2021–2060) and 2080 s (2061–2100) under SSP245 and SSP585 based on the 27 GCMs. Box boundaries indicate the 25th and 75th percentiles across GCMs, whiskers below and above the box indicate the 10th and 90th percentiles. The black lines and crosshairs within each box indicate the multi-model median and mean, respectively.

12%– 24% in three northwestern sites. Also, these trends appeared under SSP585. Furthermore, advancing sowing window could not reduce the *DHI* in the northernmost sites of Walgett and Moree Plains (Fig. 5m and Fig. 5n). The contribution of adaptation options to reduce the individual drought and heat events can be found in supplementary materials (section S2).

3.4. *The better-performing agronomic options for mitigating DH in WSP*

We selected the better-performing agronomic options corresponding to each DH indices in the 2040 s and 2080 s (Table 4 & 5). Under SSP245 and SSP585, most of the better-performing agronomic options were combined planting better-performing wheat cultivars with sowing 2 weeks earlier, and the combined options were more important in the distant future (2080 s). As for the genetic parameters of better-performing wheat cultivars in better-performing agronomic options, the TTFJ and TTFI were smaller than that of *Janz*, under two SSPs at all sites. The TTFW varied at different sites, and in most cases, it was 30°C d smaller than that of *Janz*.

Under the better-performing agronomic options, *DHF*, *DHD*, and *DHI*

Table 4
The details of the better-performing agronomic options in the 2040 s (2021–2060) and 2080 s (2061–2100) under SSP245 at six sites and the information of original management. The units for tt_end_of_juvenile (TTEJ), tt_floral_initiation (TTFI), and tt_flowering (TTFW) are all °Cd.

SSP245	Indices	Station	2040 s				2080 s			
			TTEJ	TTFI	TTFW	Sowing window	TTEJ	TTFI	TTFW	Sowing window
Better-performing agronomic options	*DHF*	Walgett	300	358	79	13 April to 1 July	300	358	79	13 April to 1 July
		Moree Plains	300	358	79	13 April to 1 July	300	358	79	13 April to 1 July
		Lachlan	300	358	79	13 April to 1 July	300	358	79	13 April to 1 July
		Mudge	300	358	79	27 April to 15 July	300	358	79	13 April to 1 July
		Balranald	300	358	169	27 April to 15 July	300	358	169	13 April to 1 July
		Wagga Wagga	300	358	79	13 April to 1 July	300	358	79	13 April to 1 July
	DHD	Walgett	300	358	79	13 April to 1 July	300	358	79	13 April to 1 July
		Moree Plains	300	358	79	20 April to 8 July	300	358	79	13 April to 1 July
		Lachlan	300	358	109	13 April to 1 July	300	358	139	13 April to 1 July
		Mudge	300	358	109	13 April to 1 July	300	358	79	13 April to 1 July
		Balranald	300	358	79	13 April to 1 July	300	358	169	13 April to 1 July
		Wagga Wagga	300	358	79	13 April to 1 July	300	358	79	13 April to 1 July
	DHI	Walgett	300	358	79	27 April to 15 July	300	358	79	13 April to 1 July
		Moree Plains	300	358	79	27 April to 15 July	300	358	79	27 April to 15 July
		Lachlan	300	358	79	13 April to 1 July	300	358	169	27 April to 15 July
		Mudge	300	358	139	27 April to 15 July	300	358	139	27 April to 15 July
		Balranald	300	358	139	27 April to 15 July	300	358	169	27 April to 15 July
		Wagga Wagga	300	358	79	13 April to 1 July	300	358	79	27 April to 15 July
Original management			400	458	109	27 April to 15 July	400	458	109	27 April to 15 July

Table 5
The details of the better-performing agronomic options in the 2040 s (2021–2060) and 2080 s (2061–2100) under SSP585 at six sites and the information of original management. The units for tt_end_of_juvenile (TTEJ), tt_floral_initiation (TTFI), and tt_flowering (TTFW) are all °Cd.

SSP585	Indices	Station	2040 s				2080 s			
			TTEJ	TTFI	TTFW	Sowing window	TTEJ	TTFI	TTFW	Sowing window
Better-performing agronomic options	*DHF*	Walgett	300	358	79	13 April to 1 July	300	358	79	13 April to 1 July
		Moree Plains	300	358	79	13 April to 1 July	300	358	79	13 April to 1 July
		Lachlan	300	358	79	13 April to 1 July	300	358	79	13 April to 1 July
		Mudge	300	358	79	27 April to 15 July	300	358	79	13 April to 1 July
		Balranald	300	358	79	27 April to 15 July	300	358	79	13 April to 1 July
		Wagga Wagga	300	358	79	13 April to 1 July	300	358	79	13 April to 1 July
	DHD	Walgett	300	358	79	13 April to 1 July	300	358	79	13 April to 1 July
		Moree Plains	300	358	79	27 April to 15 July	300	358	79	13 April to 1 July
		Lachlan	300	358	79	27 April to 15 July	300	358	79	13 April to 1 July
		Mudge	300	358	79	27 April to 15 July	300	358	109	13 April to 1 July
		Balranald	300	358	79	13 April to 1 July	300	358	109	13 April to 1 July
		Wagga Wagga	300	358	79	13 April to 1 July	300	358	109	13 April to 1 July
	DHI	Walgett	300	358	79	27 April to 15 July	300	358	79	13 April to 1 July
		Moree Plains	300	358	169	13 April to 1 July	300	358	79	27 April to 15 July
		Lachlan	300	358	79	13 April to 1 July	300	358	79	13 April to 1 July
		Mudge	300	358	79	27 April to 15 July	300	358	79	13 April to 1 July
		Balranald	300	358	79	27 April to 15 July	300	358	79	13 April to 1 July
		Wagga Wagga	300	358	79	13 April to 1 July	300	358	79	13 April to 1 July
Original management			400	458	109	27 April to 15 July	400	458	109	27 April to 15 July

in the WSP at six sites were all obviously decreased under SSP245 and SSP585 (Fig. 6). The better-performing agronomic options performed better than adjusting sowing window or planting better-performing cultivars alone (Fig. 7). They resulted in the averaged *DHF*, *DHD*, and *DHI* of six sites in 2040 s and 2080 s under SSP245 a further reduction of 10%– 16%, 14%– 17%, and 14%– 15% from adaptive measure of just planting better-performing cultivars. There was a further reduction of 25%– 40%, 25%– 41%, and 36%– 47%, respectively, from just advancing sowing window. Also, similar trends appeared under SSP585 (Fig. S5). Nevertheless, same as better-performing cultivars and ideal sowing time, better-performing agronomic options had better effects on mitigating the risk of DH in 2040 s than that in 2080 s. Taking the data under SSP245 as an example, the average *DHF* of six sites was decreased by 67% in 2040 s, but in 2080 s only by 57%. Similarly, the average *DHD* in 2040 s and 2080 s decreased by 57% and 52%, respectively, and the average *DHI* decreased by 53% and 44%, respectively. Comparing the reduction rate of DH indices among six sites, the better-performing agronomic options had the best effects at Mudgee (Fig. 6d, j, and p) and Wagga Wagga (Fig. 6f, l, and r), located in the southeast of NSW wheat belt. Specifically, under SSP245, the *DHF* of these two sites

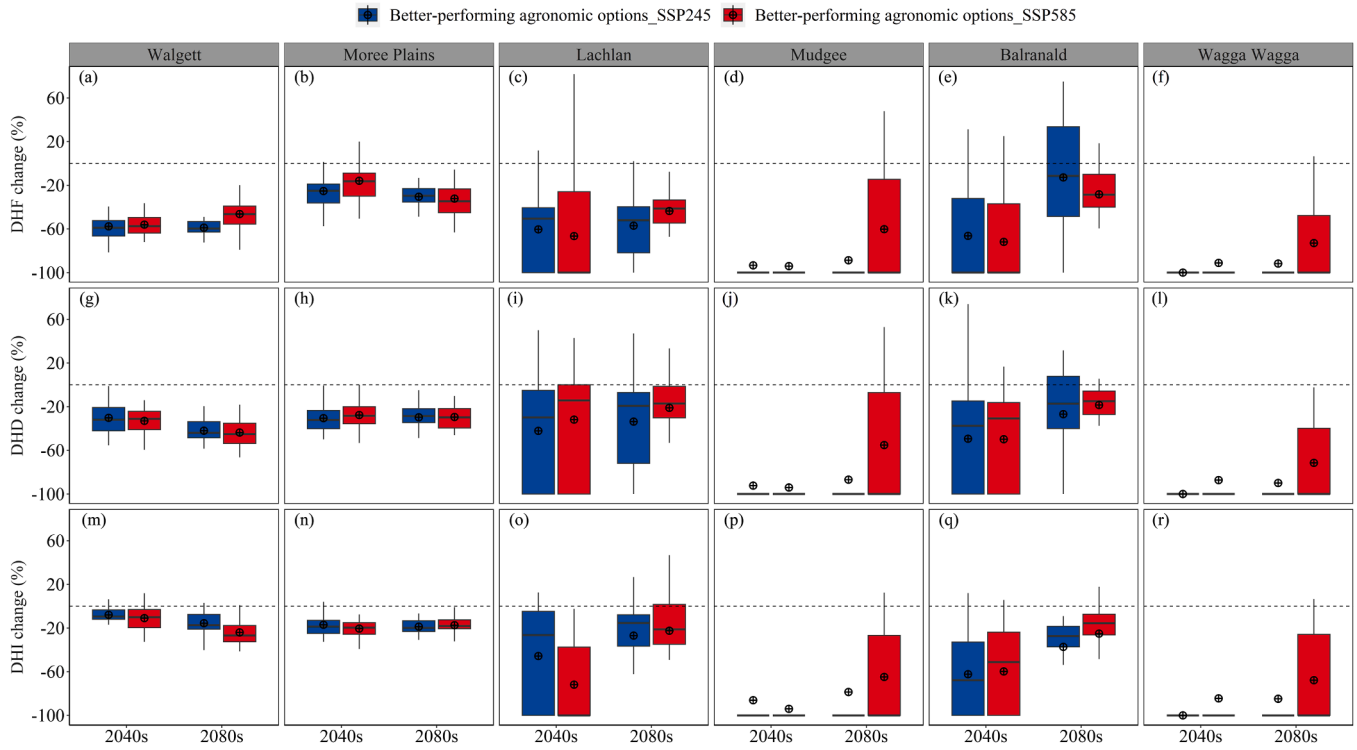

Fig. 6. Projected changes in compound drought-heat frequency (*DHF*), duration (*DHD*), and intensity (*DHI*) during the wheat sensitive period (WSP) at six sites. Changes were estimated between before and after using better-performing agronomic options for 2040 s (2021–2060) and 2080 s (2061–2100) under SSP245 and SSP585 based on the 27 downscaled GCMs. Box boundaries indicate the 25th and 75th percentiles across GCMs, whiskers below and above the box indicate the 10th and 90th percentiles. The black lines and crosshairs within each box indicate the multi-model median and mean respectively.

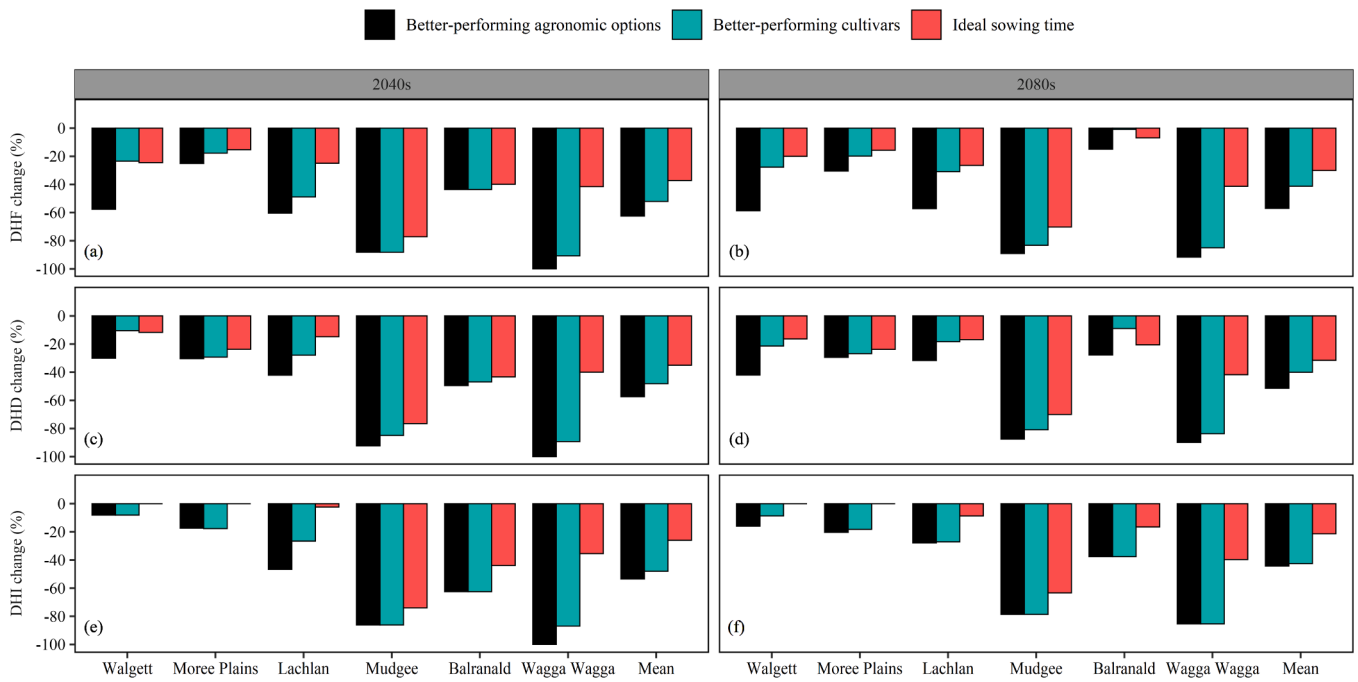

Fig. 7. Projected changes in compound drought-heat frequency (*DHF*), duration (*DHD*), and intensity (*DHI*) during the wheat sensitive period (WSP). Changes were estimated between before and after using better-performing agronomic options for 2040 s (2021–2060) and 2080 s (2061–2100) under SSP245.

decreased by 89%– 100% (Fig. 6d&f), while that of Walgett, Moree Plains, Lachlan, and Balranald decreased by 13%– 66% (Fig. 6a, b, c, and e). Similarly, the *DHD* and *DHI* decreased by 87%– 100% (Fig. 6j&l) and 79%– 100% (Fig. 6p&r) in Mudgee and Wagga Wagga, respectively, and those in the other four sites decreased by 27%– 49% (Fig. 6g, h, i, and k) and 8%– 62% respectively (Fig. 6m, n, o, and q). Similarly, the above-mentioned trends appeared under SSP585.

4. Discussion

Our study examined the effects of projected climate change on wheat flowering time using APSIM driven by multiple climate models. Under future projected climate change, the wheat flowering time was expected to be advanced at all six sites (Fig. 2). Specifically, the wheat flowering time was 5–17 days earlier in the 2040 s and 2080 s under SSP245 compared to historical period. Under SSP585, wheat flowering time was 6–27 days earlier than baseline. This was consistent with previous studies which showed that simulated days to flowering were shortened under future climate due to global warming (Wang et al., 2017a; Zheng et al., 2012). Wheat flowering time advanced from the middle or late September in the 2000 s to the middle or late August in the 2040 s and 2080 s under projected climate change. Additionally, we found that *DHF*, *DHD*, and *DHI* almost all increased in the future (Fig. 3), which is consistent with the results of previous studies. For example, Sedlmeier et al. (2018) and Zhou et al. (2019) reported that the frequency, intensity, and influenced area of DH events are all increased in the warm season. Besides, we found that drought events in WSP would not change too much in the future (Fig. S3) while heat events would clearly increase (Fig. S4). Therefore, the increase in DH events was mainly due to the increase in heat stress, which is consistent with the findings of Zhang et al. (2022), who reported the increased temperature dominated the increase in DH events. The reason may be that drought is a recurring climate feature in Australia (Ummenhofer et al., 2009), and the drought frequency, duration, and intensity are at a high level (Fig. S3). In this case, when heat becomes more frequent, more DH events will occur.

Spatially, we found that in Walgett and Moree Plains, located in the northern NSW wheat belt, the increases of *DHF* and *DHD* in the future were larger than that at the other four sites in the central and southern part of the wheat belt, Lachlan, Mudgee, Balranald, and Wagga Wagga (Fig. 3). The reason is that these two northern sites have a higher temperature. Specifically, the average daily maximum temperature in the wheat growing season in Walgett and Moree Plains is 2.3–4.8 ℃ higher than that in Lachlan, Mudgee, Balranald, and Wagga Wagga (Table 1). Coupled with the gradual warming climate in the future, the frequency and duration of heat in Walgett and Moree Plains would be higher than those in the other four sites (Fig. S4). Meanwhile, the drought frequency and duration were also high in Walgett and Moree Plains (Fig. S3). Therefore, in the case of a significant increase in heat events and frequent drought events, DH events naturally occur more frequently in the two sites. By contrast, for Lachlan, Mudgee, Balranald, and Wagga Wagga, which are located in the middle to the south of the wheat belt, the *DHF* and *DHD* did not increase much in the future. The reason is that the wheat flowering time in these sites was more advanced in the future (Fig. 2), helping wheat escape the DH events under projected climate change during the flowering period. In addition, the *DHI* in Balranald was the highest among all sites. This is because Balranald is the driest site with the largest drought intensity (Fig. S3) located in the westernmost area. In summary, DH events are prone to occur in the north and west of the wheat belt, and the frequency, duration, and intensity of DH events would increase in the future.

Additionally, we tested the potential of single and combined agronomic options in alleviating DH events. We adopted two adaptation practices, changing sowing time and wheat cultivars. Such agronomic options are cost-friendly and easily adopted by farmers. We discovered that either single or combined agronomic options would be effective in reducing *DHF*, *DHD*, and *DHI* in WSP (Figs. 3–5). We found that better-performing wheat cultivars under future climate had a shorter vegetative period compared to reference cultivar, *Janz*. Also, this is consistent with Devasirvatham et al. (2016) and Wang et al. (2019), who proposed that early flowering wheat has a higher resilience to extreme weather events. We found that both better-performing cultivars and ideal sowing time promote wheat to flower earlier than the original mid-spring, keeping the sensitive flowering period in a cooler season. With the decrease of heat stress in the cooler season, the risk of DH also decreases, even though the NSW wheat belt is prone to drought in spring and winter (Feng et al., 2019a). On the basis of planting early flowering

wheat, advancing the sowing time can further promote wheat flowering earlier and ensure the sensitive flowering period is completed prior to frequent DH events, thus escaping DH events to a greater extent.

Although adopting early time of sowing and early flowering cultivar under future climate can significantly reduce the DH risks during WSP, there might also be yield penalties or other climatic risks. Adopting early flowering wheat cultivar would shorten the length of the vegetative season, leading to the reduction of the growth period to intercept the radiation, nutrition, and CO_2 for the accumulation of photosynthate, which affects biomass accumulation and yield formation (Zheng et al., 2012; García et al., 2018). In contrast, it is generally believed that early sowing the wheat with suitable maturity time can boost wheat yield (Hunt et al., 2019; Kerr et al., 1992), but it should be no earlier than mid-April. The main reason is the greater competition for assimilates between the growing spike and the elongating stem (Gomez-Macpherson and Richards, 1995). The combination of the two adaptations may make the adverse effects stronger. However, these adverse impacts can be overcome by genetically prolonging the grain filling stage and shortening the stems of winter wheat (Gomez-Macpherson and Richards, 1995; Kerr et al., 1992).

In addition to agronomic options aimed at escaping DH events, other options focused on enhancing the tolerance of wheat to drought and heat stress may also have the potential to alleviate the adverse impacts resulting from DH events. For instance, the options of genetic improvement of wheat to drought and heat stress, straw or residue mulching, soil management techniques, appropriate amount and methods of fertilization, and the application of exogenous protectants, etc. These options can improve both crop water and nutrient use efficiency and increase soil moisture retention (Akter and Rafiqul Islam, 2017; Dodd et al., 2011). Therefore, it is imperative to explore and validate the effectiveness of these agronomic options to escape DH events in future work.

Furthermore, we found that the frost risks were increased in the 2040 s and 2080 s across six sites under SSP245 and SSP585 under the optimal agronomic options. This increase was particularly notable in regions with climates that are less dry and hot, such as Mudgee and Wagga Wagga (Fig. S10). Specifically, frost frequency (FF) at Mudgee was increased by 2%− 77% in the 2040 s and 2080 s under two scenarios. Frost intensity (FI) increased by 62%− 88% at Wagga Wagga. By combining frost-tolerant traits in wheat cultivars or implementing protective measures such as delving of surfaced soils, the negative impacts of increased frosts may be further reduced (Farre et al., 2003; Rebbeck et al., 2007; Zheng et al., 2015). Although our optimal agronomic options demonstrate a significant reduction in DH risks by 89%− 100% at two southeastern sites of Mudgee and Wagga Wagga, these options also resulted in a notable increase in the risk of frost during WSP. Therefore, farmers and decision-makers should carefully consider local climate conditions and frost patterns when determining suitable agronomic options, especially for regions that are characterized by less dry-hot climates. Additionally, it's worth noting that our suggested agronomic options did not greatly increase the exposure of wheat to spring frosts at four other sites, making them viable choices for regions with dry-hot climates.

For the first time, we defined compound DH events in WSP and assessed the characteristics of DH events under projected climate change in southeastern Australia's wheat growing regions. Our results can provide important information for better management of climate risk within the grain industry, but there are still limitations to our approach. First, similar with previous studies on adaptation of wheat to projected climate change (Semenov et al., 2014; Wang et al., 2019), we only changed sowing time and cultivar, but did not consider other strategies to increase soil moisture. For example, residue retention and straw mulching are demonstrated to reduce soil surface evaporation, which is beneficial to the wheat growth in Australia (Dang et al., 2006; Hunt et al., 2013). However, they are not included in our study due to the heavy calculation load caused by the many agronomic option combinations. Second, we only used one crop model. Recently, multiple crop model ensembles provided more robust results than single models in simulating crop growth and development (Rötter et al., 2015). Tao et al. (2017) designed ideal crop genotypes based on multi-model ensembles. We acknowledge that our results relied on the simulations of APSIM model. Further works with multiple crop model comparisons are needed to reduce the uncertainty in research results. Third, we only considered the simultaneous drought and heat stresses during wheat flowing period. However, the risk of frost in late spring is also non-negligible for Australian wheat (Wang et al., 2015b; Zheng et al., 2012). Therefore, it is necessary to consider more extreme climate events to study the compound and interaction of multiple hazards as comprehensively as possible.

5. Conclusion

We developed the compound drought-heat index to assess the occurrences of simultaneous water and heat stresses during WSP under the expected effects of climate change in Australia. We found that the *DHF*, *DHD*, and *DHI* in WSP were projected to increase by 15%, 12%, and 0.9% in 2040 s, and 49%, 44%, and 5% in 2080 s, respectively, averaged across six sites compared with baseline climate. The increased DH events were mainly due to the increase in heat stress, especially at sites located in the northern NSW wheat belt with dry-hot climate. In addition, we demonstrated the adaptative effects of early sowing and wheat cultivars with shorter vegetative phase on reducing the risk of DH events. These agronomic options facilitated wheat to escape the jeopardizing effects of compound drought-heat events under projected climate change at study sites. However, they may introduce an increased frost risk across six study sites, especially in regions with climates that are less dry and hot, such as Mudgee and Wagga Wagga. We believe that our study will provide helpful information for farmers in Australia to mitigate the adverse effects of extreme climate events on wheat. The framework we developed here can be extended to other dryland wheat growing regions globally.

CRediT authorship contribution statement

Siyi Li: Conceptualization, Methodology, Software, Writing – original draft, Formal analysis, Visualization. **Bin Wang:** Conceptualization, Methodology, Writing – review & editing, Investigation, Supervision. **De Li Liu:** Conceptualization, Software, Supervision, Data Curation, Writing – review & editing. **Chao Chen**: Methodology, Writing – review & editing. **Puyu Feng:** Software, Writing – review & editing. **Mingxia Huang:** Software. **Xiaofang Wang:** Methodology. **Lijie Shi:** Writing – review & editing, **Cathy Waters:** Project administration, **Alfredo Huete:** Supervision, Writing – review & editing. **Qiang Yu:** Methodology, Supervision.

Declaration of Competing Interest

The authors declare that they have no known competing financial interests or personal relationships that could have appeared to influence the work reported in this paper.

Data Availability

Data will be made available on request.

Acknowledgements

The first author acknowledges the China Scholarship Council (CSC) for the financial support for her Ph.D. study. Facilities for conducting this study were provided by the New South Wales Department of Primary Industries. Dr. Bernie Dominiak provided comments on an earlier version of this manuscript. We acknowledge the World Climate Research

Programme, which, through its Working Group on Coupled Modelling, coordinated and promoted CMIP6. We thank the climate modeling groups for producing and making available their model output, the Earth System Grid Federation (ESGF) for archiving the data and providing access, and the multiple funding agencies who support CMIP6 and ESGF. We are very grateful to two reviewers for their very thorough and helpful comments which greatly improved our manuscript.

Appendix A. Supporting information

Supplementary data associated with this article can be found in the online version at doi:10.1016/j.eja.2023.127030.

References

Ababaei, B., Chenu, K., 2020. Heat shocks increasingly impede grain filling but have little effect on grain setting across the Australian wheatbelt. Agric. For. Meteorol. 284, 107889.
Akter, N., Rafiqul Islam, M., 2017. Heat stress effects and management in wheat. A review. Agron. Sustain. Dev. 37 (5), 37.
Alexander, B., Hayman, P., McDonald, G., Talukder, H., Gill, G., 2010. Characterising the risk of heat stress on wheat in South Australia: meteorology, climatology and the design of a field heating chamber. Proc. 15th Aust. Agron. Conf., Linc., N. Z.
Amarasingha, R.P.R.K., Suriyagoda, L.D.B., Marambe, B., Gaydon, D.S., Galagedara, L. W., Punyawardena, R., Silva, G.L.L.P., Nidumolu, U., Howden, M., 2015. Simulation of crop and water productivity for rice (Oryza sativa L.) using APSIM under diverse agro-climatic conditions and water management techniques in Sri Lanka. Agric. Water Manag. 160, 132–143.
Anwar, M.R., Liu, D.L., Farquharson, R., Macadam, I., Abadi, A., Finlayson, J., Wang, B., Ramilan, T., 2015. Climate change impacts on phenology and yields of five broadacre crops at four climatologically distinct locations in Australia. Agric. Syst. 132, 133–144.
APSIM, 2015. The APSIM-Wheat Module (7.5 R3008).
Archontoulis, S.V., Miguez, F.E., Moore, K.J., 2014. Evaluating APSIM maize, soil water, soil nitrogen, manure, and soil temperature modules in the midwestern United States. Agron. J. 106, 1025–1040.
Asseng, S., van Keulen, H., Stol, W., 2000. Performance and application of the APSIM Nwheat model in the Netherlands. Eur. J. Agron. 12, 37–54.
Asseng, S., Turner, N.C., Keating, B.A., 2001. Analysis of water-and nitrogen-use efficiency of wheat in a Mediterranean climate. Plant Soil 233, 127–143.
Asseng, S., Foster, I.A.N., Turner, N.C., 2011. The impact of temperature variability on wheat yields. Glob. Change Biol. 17, 997–1012.
Bastos, A., Ciais, P., Friedlingstein, P., Sitch, S., Pongratz, J., Fan, L., Wigneron, J.P., Weber, U., Reichstein, M., Fu, Z., Anthoni, P., Arneth, A., Haverd, V., Jain, A.K., Joetzjer, E., Knauer, J., Lienert, S., Loughran, T., McGuire, P.C., Tian, H., Viovy, N., Zaehle, S., 2020. Direct and seasonal legacy effects of the 2018 heat wave and drought on European ecosystem productivity. Sci. Adv. 6, eaba2724.
Chen, Y.L., Palta, J., Clements, J., Buirchell, B., Siddique, K.H.M., Rengel, Z., 2014. Root architecture alteration of narrow-leafed lupin and wheat in response to soil compaction. Field Crops Res. 165, 61–70.
Chenu, K., Cooper, M., Hammer, G.L., Mathews, K.L., Dreccer, M.F., Chapman, S.C., 2011. Environment characterization as an aid to wheat improvement: interpreting genotype–environment interactions by modelling water-deficit patterns in North-Eastern Australia. J. Exp. Bot. 62, 1743–1755.
Chenu, K., Deihimfard, R., Chapman, S.C., 2013. Large-scale characterization of drought pattern: a continent-wide modelling approach applied to the Australian wheatbelt – spatial and temporal trends. N. Phytol. 198, 801–820.
Ciais, P., Reichstein, M., Viovy, N., Granier, A., Ogée, J., Allard, V., Aubinet, M., Buchmann, N., Bernhofer, C., Carrara, A., Chevallier, F., De Noblet, N., Friend, A.D., Friedlingstein, P., Grünwald, T., Heinesch, B., Keronen, P., Knohl, A., Krinner, G., Loustau, D., Manca, G., Matteucci, G., Miglietta, F., Ourcival, J.M., Papale, D., Pilegaard, K., Rambal, S., Seufert, G., Soussana, J.F., Sanz, M.J., Schulze, E.D., Vesala, T., Valentini, R., 2005. Europe-wide reduction in primary productivity caused by the heat and drought in 2003. Nature 437, 529–533.
Cohen, I., Zandalinas, S.I., Huck, C., Fritschi, F.B., Mittler, R.J.P.P., 2021. Meta-analysis of drought and heat stress combination impact on crop yield and yield components. Physiol. Plant. 171, 66–76.
Cossani, C.M., Slafer, G.A., Savin, R., 2009. Yield and biomass in wheat and barley under a range of conditions in a Mediterranean site. Field Crops Res. 112, 205–213.
Dalgliesh, N., Cocks, B., Horan, H., 2012. APSoil-providing soils information to consultants, farmers and researchers. 16th Aust. Agron. Conf., Armidale, NSW.
Dang, Y.P., Dalal, R.C., Routley, R., Schwenke, G.D., Daniells, I., 2006. Subsoil constraints to grain production in the cropping soils of the north-eastern region of Australia: an overview. Aust. J. Exp. Agric. 46, 19–35.
Devasirvatham, V., Tan, D.K., Trethowan, R.M., 2016. Breeding strategies for enhanced plant tolerance to heat stress, Advances in plant breeding strategies: agronomic, abiotic and biotic stress traits. Springer, pp. 447–469.
Dias, A.S., Lidon, F.C., 2009. Evaluation of Grain Filling Rate and Duration in Bread and Durum Wheat, under Heat Stress after Anthesis. J. Agron. Crop Sci. 195, 137–147.
Dodd, I.C., Whalley, W.R., Ober, E.S., Parry, M.A.J., 2011. Genetic and management approaches to boost UK wheat yields by ameliorating water deficits. J. Exp. Bot. 62 (15), 5241–5248.
Dodd, R.J., Chadwick, D.R., Harris, I.M., Hines, A., Hollis, D., Economou, T., Gwynn-Jones, D., Scullion, J., Robinson, D.A., Jones, D.L., 2021. Spatial co-localisation of extreme weather events: a clear and present danger. Ecol. Lett. 24, 60–72.
Elahi, E., Khalid, Z., Tauni, M.Z., Zhang, H., Lirong, X.J.T., 2021. Extreme weather events risk to crop-production and the adaptation of innovative management strategies to mitigate the risk: a retrospective survey of rural Punjab. Pak. Technovation, 102255.
Fan, J., McConkey, B., Wang, H., Janzen, H., 2016. Root distribution by depth for temperate agricultural crops. Field Crops Res. 189, 68–74.
FAO, 2021. The Food and Agriculture Organization of the United Nations. Statistic data base. ⟨https://www.fao.org/faostat/en/#data/QCL⟩.
Farre, I., Foster, I., Biddulph, B., Asseng, S., 2003. Is there a value in having a frost forecast for wheat in the South-West of Western Australia.
Feng, P., Liu, D.L., Wang, B., Waters, C., Zhang, M., Yu, Q., 2019a. Projected changes in drought across the wheat belt of southeastern Australia using a downscaled climate ensemble. Int. J. Climatol. 39, 1041–1053.
Feng, P., Wang, B., Liu, D.L., Waters, C., Xiao, D., Shi, L., Yu, Q., 2020. Dynamic wheat yield forecasts are improved by a hybrid approach using a biophysical model and machine learning technique. Agric. For. Meteorol. 285–286, 107922.
Feng, S., Hao, Z., Zhang, X., Hao, F., 2019b. Probabilistic evaluation of the impact of compound dry-hot events on global maize yields. Sci. Total Environ. 689, 1228–1234.
Flohr, B.M., Hunt, J.R., Kirkegaard, J.A., Evans, J.R., Lilley, J.M., 2018. Genotype × management strategies to stabilise the flowering time of wheat in the south-eastern Australian wheatbelt. Crop Pasture Sci. 69, 547–560.
Frank, A.B., Bauer, A., 1982. Effect of temperature and fertilizer N on apex development in spring wheat1. Agron. J. 74, 504–509.
Gan, Y., Liu, L., Cutforth, H., Wang, X., Ford, G., 2011. Vertical distribution profiles and temporal growth patterns of roots in selected oilseeds, pulses and spring wheat. Crop and Pasture. Science 62, 457–466.
García, G.A., Miralles, D.J., Serrago, R.A., Alzueta, I., Huth, N., Dreccer, M.F., 2018. Warm nights in the Argentine Pampas: Modelling its impact on wheat and barley shows yield reductions. Agric. Syst. 162, 259–268.
Geirinhas, J.L., Russo, A., Libonati, R., Sousa, P.M., Miralles, D.G., Trigo, R.M., 2021. Recent increasing frequency of compound summer drought and heatwaves in Southeast Brazil. Environ. Res. Lett. 16, 034036.
Giraldo, P., Benavente, E., Manzano-Agugliaro, F., Gimenez, E., 2019. Worldwide research trends on wheat and barley: a bibliometric comparative analysis. Agronomy 9, 352.
Gomez-Macpherson, H., Richards, R.A., 1995. Effect of sowing time on yield and agronomic characteristics of wheat in south-eastern Australia. Aust. J. Agric. Res. 46, 1381–1399.
Gouache, D., Le Bris, X., Bogard, M., Deudon, O., Pagé, C., Gate, P., 2012. Evaluating agronomic adaptation options to increasing heat stress under climate change during wheat grain filling in France. Eur. J. Agron. 39, 62–70.
Granier, A., Bréda, N., Biron, P., Villette, S., 1999. A lumped water balance model to evaluate duration and intensity of drought constraints in forest stands. Ecol. Model. 116, 269–283.
Grose, M.R., Narsey, S., Delage, F.P., Dowdy, A.J., Bador, M., Boschat, G., Chung, C., Kajtar, J.B., Rauniyar, S., Freund, M.B., Lyu, K., Rashid, H., Zhang, X., Wales, S., Trenham, C., Holbrook, N.J., Cowan, T., Alexander, L., Arblaster, J.M., Power, S., 2020. Insights from CMIP6 for Australia's future climate. Earth'S. Future 8 e2019EF001469.
Guo, Y., Lu, X., Zhang, J., Li, K., Wang, R., Rong, G., Liu, X., Tong, Z., 2022. Joint analysis of drought and heat events during maize (Zea mays L.) growth periods using copula and cloud models: a case study of Songliao Plain. Agric. Water Manag. 259, 107238.
Hao, S., Ryu, D., Western, A., Perry, E., Bogena, H., Franssen, H.J.H., 2021. Performance of a wheat yield prediction model and factors influencing the performance: a review and meta-analysis. Agric. Syst. 194, 103278.
Hasanuzzaman, M., Fujita, M., 2011. Selenium pretreatment upregulates the antioxidant defense and methylglyoxal detoxification system and confers enhanced tolerance to drought stress in rapeseed seedlings. Biol. Trace Elem. Res. 143 (3), 1758–1776.
Holzworth, D.P., Huth, N.I., deVoil, P.G., Zurcher, E.J., Herrmann, N.I., McLean, G., Chenu, K., van Oosterom, E.J., Snow, V., Murphy, C.J.E.M., Software, 2014. APSIM–evolution towards a new generation of agricultural systems simulation. Environ. Model. Softw. 62, 327–350.
Hunt, J.R., Browne, C., McBeath, T.M., Verburg, K., Craig, S., Whitbread, A.M., 2013. Summer fallow weed control and residue management impacts on winter crop yield though soil water and N accumulation in a winter-dominant, low rainfall region of southern Australia. Crop Pasture Sci. 64, 922–934.
Hunt, J.R., Lilley, J.M., Trevaskis, B., Flohr, B.M., Peake, A., Fletcher, A., Zwart, A.B., Gobbett, D., Kirkegaard, J.A., 2019. Early sowing systems can boost Australian wheat yields despite recent climate change. Nat. Clim. Change 9, 244–247.
Innes, P.J., Tan, D.K.Y., Van Ogtrop, F., Amthor, J.S., 2015. Effects of high-temperature episodes on wheat yields in New South Wales, Australia. Agric. For. Meteorol. 208, 95–107.
Jones, C.A., Kiniry, J.R., 1986. A simulation model of maize growth and development. Texas A & M University Press, College Station.
Keating, B.A., Carberry, P.S., Hammer, G.L., Probert, M.E., Robertson, M.J., Holzworth, D., Huth, N.I., Hargreaves, J.N.G., Meinke, H., Hochman, Z., McLean, G., Verburg, K., Snow, V., Dimes, J.P., Silburn, M., Wang, E., Brown, S., Bristow, K.L., Asseng, S., Chapman, S., McCown, R.L., Freebairn, D.M., Smith, C.J., 2003. An overview of APSIM, a model designed for farming systems simulation. Eur. J. Agron. 18, 267–288.

Kerr, N.J., Siddique, K.H.M., Delane, R.J., 1992. Early sowing with wheat cultivars of suitable maturity increases grain yield of spring wheat in a short season environment. Aust. J. Exp. Agric. 32, 717–723.
Kirkegaard, J.A., Lilley, J.M., 2007. Root penetration rate a benchmark to identify soil and plant limitations to rooting depth in wheat. Aust. J. Exp. Agric. Aust. J. Exp. Agric. 47, 590–602.
Kong, Q., Guerreiro, S.B., Blenkinsop, S., Li, X.-F., Fowler, H.J., 2020. Increases in summertime concurrent drought and heatwave in Eastern China. Weather Clim. Extrem. 28, 100242.
Korres, N.E., Norsworthy, J.K., Burgos, N.R., Oosterhuis, D.M., 2017. Temperature and drought impacts on rice production: An agronomic perspective regarding short- and long-term adaptation measures. Water Resour. Rural Dev. 9, 12–27.
Kumar Tewari, A., Charan Tripathy, B., 1998. Temperature-Stress-Induced Impairment of Chlorophyll Biosynthetic Reactions in Cucumber and Wheat1. Plant Physiol. 117, 851–858.
Lalic, B., Eitzinger, J., Mihailovic, D.T., Thaler, S., Jancic, M., 2013. Climate change impacts on winter wheat yield change–which climatic parameters are crucial in Pannonian lowland? J. Agric. Sci. 151, 757–774.
Lesk, C., Rowhani, P., Ramankutty, N., 2016. Influence of extreme weather disasters on global crop production. Nature 529, 84–87.
Lesk, C., Coffel, E., Winter, J., Ray, D., Zscheischler, J., Seneviratne, S.I., Horton, R., 2021. Stronger temperature–moisture couplings exacerbate the impact of climate warming on global crop yields. Nat. Food 2, 683–691.
Li, S.Y., Miao, L.J., Jiang, Z.H., Wang, G.J., Gnyawali, K.R., Zhang, J., Zhang, H., Fang, K., He, Y., Li, C., 2020. Projected drought conditions in Northwest China with CMIP6 models under combined SSPs and RCPs for 2015–2099. Adv. Clim. Change Res. 11, 210–217.
Li, E., Zhao, J., Pullens, J.W.M., Yang, X., 2022. The compound effects of drought and high temperature stresses will be the main constraints on maize yield in Northeast China. Sci. Total Environ. 812, 152461.
Littleboy, M., Silburn, D., Freebairn, D., Woodruff, D., Hammer, G., Leslie, J., 1992. Impact of soil erosion on production in cropping systems. I. Development and validation of a simulation model. Aust. J. Soil Res. 30, 757–774.
Liu, D.L., 2007. Incorporating vernalization response functions into an additive phenological model for reanalysis of the flowering data of annual pasture legumes. Field Crops Res. 101, 331–342.
Liu, D.L., Zuo, H., 2012. Statistical downscaling of daily climate variables for climate change impact assessment over New South Wales, Australia. Clim. Change 115, 629–666.
Liu, D.L., Anwar, M.R., O'Leary, G., Conyers, M.K., 2014. Managing wheat stubble as an effective approach to sequester soil carbon in a semi-arid environment: Spatial modelling. Geoderma 214–215, 50–61.
Lobell, D.B., Hammer, G.L., Chenu, K., Zheng, B., McLean, G., Chapman, S.C., 2015. The shifting influence of drought and heat stress for crops in northeast Australia. Glob. Change Biol. 21, 4115–4127.
Madadgar, S., AghaKouchak, A., Farahmand, A., Davis, S.J., 2017. Probabilistic estimates of drought impacts on agricultural production. Geophys. Res. Lett. 44, 7799–7807.
Manavalan, L.P., Guttikonda, S.K., Phan Tran, L.-S., Nguyen, H.T., 2009. Physiological and molecular approaches to improve drought resistance in soybean. Plant Cell Physiol. 50 (7), 1260–1276.
Maqbool, M.A., Aslam, M., Ali, H., 2017. Breeding for improved drought tolerance in Chickpea (Cicer arietinum L.). Plant Breed. 136 (3), 300–318.
Mohi-Ud-Din, M., Siddiqui, N., Rohman, M., Jagadish, S.V.K., Ahmed, J.U., Hassan, M. M., Hossain, A., Islam, T., 2021. Physiological and biochemical dissection reveals a trade-off between antioxidant capacity and heat tolerance in bread wheat (Triticum aestivum L.). Antioxidants 10 (3), 351.
Mondal, S., Singh, R.P., Huerta-Espino, J., Kehel, Z., Autrique, E., 2015. Characterization of heat- and drought-stress tolerance in high-yielding spring wheat. Crop Sci. 55 (4), 1552–1562.
Mukherjee, S., Ashfaq, M., Mishra, A.K., 2020. Compound drought and heatwaves at a global scale: the role of natural climate variability-associated synoptic patterns and land-surface energy budget anomalies. J. Geophys. Res.: Atmosph. 125 e2019JD031943.
Mukherjee, S., Mishra, A.K., 2021. Increase in compound drought and heatwaves in a warming world. Geophys. Res. Lett. 48 e2020GL090617.
Mullarkey, M., Jones, P., 2000. Isolation and analysis of thermotolerant mutants of wheat. J. Exp. Bot. 51, 139–146.
Pimstein, A., Eitel, J.U.H., Long, D.S., Mufradi, I., Karnieli, A., Bonfil, D.J., 2009. A spectral index to monitor the head-emergence of wheat in semi-arid conditions. Field Crops Res. 111 (3), 218–225.
Pirttioja, N., Palosuo, T., Fronzek, S., Räisänen, J., Rötter, R.P., Carter, T.R., 2019. Using impact response surfaces to analyse the likelihood of impacts on crop yield under probabilistic climate change. Agric. For. Meteorol. 264, 213–224.
Porter, J.R., Gawith, M., 1999. Temperatures and the growth and development of wheat: a review. Eur. J. Agron. 10, 23–36.
Poudel, P.B., Poudel, M.R., 2020. Heat stress effects and tolerance in wheat: A review. J. Biol. Today'S. World 9, 1–6.
Prasad, P.V.V., Staggenborg, S.A., Ristic, Z., 2008. Impacts of drought and/or heat stress on physiological, developmental, growth, and yield processes of crop plants. In Response of Crops to Limited Water. In: Ahuja, L.H., Saseendran, S.A. (Eds.), Advances in Agricultural Systems Modeling Series 1, 2008. ASA-CSSA, Madison, WI, USA, pp. 301–355.
Rawson, H., Bagga, A., 1979. Influence of temperature between floral initiation and flag leaf emergence on grain number in wheat. Aust. J. Plant Physiol. 6, 391–400.
Rebbeck, M., Lynch, C., Hayman, P.T., Sadras, V.O., 2007. Delving of sandy surfaced soils reduces frost damage in wheat crops. Aust. J. Agric. Res. 58, 105–112.
Ribeiro, A.F.S., Russo, A., Gouveia, C.M., Páscoa, P., Zscheischler, J.J.B., 2020. Risk of crop failure due to compound dry and hot extremes estimated with nested copulas. Biogeosciences 17, 4815–4830.
Richardson, C.W., Wright, D.A., 1984. A model for generating daily weather variables. United States Department of Agriculture. Agriculture Research Service,, Washington, DC, USA, pp. 1–86.
Ristic, Z., Bukovnik, U., Prasad, P.V.V., 2007. Correlation between heat stability of thylakoid membranes and loss of chlorophyll in winter wheat under heat stress. Crop Sci. 47, 2067–2073.
Rötter, R.P., Tao, F., Höhn, J.G., Palosuo, T., 2015. Use of crop simulation modelling to aid ideotype design of future cereal cultivars. J. Exp. Bot. 66, 3463–3476.
Saini, H.S., Westgate, M.E., 1999. Reproductive development in grain crops during drought. Adv. Agron. 68, 59–96.
Sedlmeier, K., Feldmann, H., Schädler, G., 2018. Compound summer temperature and precipitation extremes over central Europe. Theor. Appl. Climatol. 131, 1493–1501.
Semenov, M.A., Stratonovitch, P., 2015. Adapting wheat ideotypes for climate change: accounting for uncertainties in CMIP5 climate projections. Clim. Res. 65, 123–139.
Semenov, M.A., Stratonovitch, P., Alghabari, F., Gooding, M.J., 2014. Adapting wheat in Europe for climate change. J. Cereal Sci. 59, 245–256.
Seyoum, S., Chauhan, Y., Rachaputi, R., Fekybelu, S., Prasanna, B., 2017. Characterising production environments for maize in eastern and southern Africa using the APSIM Model. Agric. For. Meteorol. 247, 445–453.
Shah, N.H., Paulsen, G.M., 2003. Interaction of drought and high temperature on photosynthesis and grain-filling of wheat. Plant Soil 257, 219–226.
Stratonovitch, P., Semenov, M.A., 2015. Heat tolerance around flowering in wheat identified as a key trait for increased yield potential in Europe under climate change. J. Exp. Bot. 66, 3599–3609.
Talukder, A.S.M.H.M., McDonald, G.K., Gill, G.S., 2013. Effect of short-term heat stress prior to flowering and at early grain set on the utilization of water-soluble carbohydrate by wheat genotypes. Field Crops Res. 147, 1–11.
Talukder, A.S.M.H.M., McDonald, G.K., Gill, G.S., 2014. Effect of short-term heat stress prior to flowering and early grain set on the grain yield of wheat. Field Crops Res. 160, 54–63.
Tao, F., Rötter, R.P., Palosuo, T., Díaz-Ambrona, C.G.H., Mínguez, M.I., Semenov, M.A., Kersebaum, K.C., Nendel, C., Cammarano, D., Hoffmann, H., Ewert, F., Dambreville, A., Martre, P., Rodríguez, L., Ruiz-Ramos, M., Gaiser, T., Höhn, J.G., Salo, T., Ferrise, R., Bindi, M., Schulman, A.H., 2017. Designing future barley ideotypes using a crop model ensemble. Eur. J. Agron. 82, 144–162.
Tashiro, T., Wardlaw, I., 1990. The response to high temperature shock and humidity changes prior to and during the early stages of grain development in wheat. Aust. J. Plant Physiol. 17, 551–561.
Turner, N.C., 1980. Turgor maintenance by osmotic adjustment: a review and evaluation. Adapt. Plants Water High. Temp. Stress 87–103.
Ummenhofer, C.C., England, M.H., McIntosh, P.C., Meyers, G.A., Pook, M.J., Risbey, J.S., Gupta, A.S., Taschetto, A.S., 2009. What causes southeast Australia's worst droughts? Geophys. Res. Lett. 36.
Vignjevic, M., Wang, X., Olesen, J.E., Wollenweber, B., 2015. Traits in spring wheat cultivars associated with yield loss caused by a heat stress episode after anthesis. J. Agron. Crop Sci. 201, 32–48.
Vogel, E., Donat, M.G., Alexander, L.V., Meinshausen, M., Ray, D.K., Karoly, D., Meinshausen, N., Frieler, K., 2019. The effects of climate extremes on global agricultural yields. Environ. Res. Lett. 14, 054010.
Wang, B., Chen, C., Li Liu, D., Asseng, S., Yu, Q., Yang, X., 2015a. Effects of climate trends and variability on wheat yield variability in eastern Australia. Clim. Res. 64, 173–186.
Wang, B., Liu, D.L., Asseng, S., Macadam, I., Yu, Q., 2015b. Impact of climate change on wheat flowering time in eastern Australia. Agric. For. Meteorol. 209–210, 11–21.
Wang, B., Liu, D.L., Asseng, S., Macadam, I., Yang, X., Yu, Q., 2017a. Spatiotemporal changes in wheat phenology, yield and water use efficiency under the CMIP5 multimodel ensemble projections in eastern Australia. Clim. Res. 72, 83–99.
Wang, B., Liu, D.L., Asseng, S., Macadam, I., Yu, Q., 2017b. Modelling wheat yield change under CO_2 increase, heat and water stress in relation to plant available water capacity in eastern Australia. Eur. J. Agron. 90, 152–161.
Wang, B., Feng, P., Chen, C., Liu, D.L., Waters, C., Yu, Q., 2019. Designing wheat ideotypes to cope with future changing climate in South-Eastern Australia. Agric. Syst. 170, 9–18.
Wang, C., Li, Z., Chen, Y., Li, Y., Liu, X., Hou, Y., Wang, X., Kulaixi, Z., Sun, F., 2022. Increased compound droughts and heatwaves in a double pack in Central Asia. Remote Sens. 14, 2959.
Wang, J., Wang, E., Luo, Q., Kirby, M., 2009. Modelling the sensitivity of wheat growth and water balance to climate change in Southeast Australia. Clim. Change 96, 79–96.
Wenda-Piesik, A., 2011. Volatile organic compound emissions by winter wheat plants (Triticum aestivum L.) under Fusarium spp. Infestation and various abiotic conditions. Pol. J. Environ. Stud. 20.
Wheeler, T.R., Batts, G.R., Ellis, R.H., Hadley, P., Morison, J.I.L., 1996. Growth and yield of winter wheat (Triticum aestivum) crops in response to CO_2 and temperature. J. Agric. Sci. 127, 37–48.
Xiao, D., Liu, D.L., Wang, B., Feng, P., Waters, C., 2020. Designing high-yielding maize ideotypes to adapt changing climate in the North China Plain. Agric. Syst. 181, 102805.
Yang, X., Zhou, B., Xu, Y., Han, Z., 2021. CMIP6 evaluation and projection of temperature and precipitation over China. Adv. Atmos. Sci. 38, 817–830.
You, Q., Cai, Z., Wu, F., Jiang, Z., Pepin, N., Shen, S.S.P., 2021. Temperature dataset of CMIP6 models over China: evaluation, trend and uncertainty. Clim. Dyn. 57, 17–35.
Zadoks, J.C., Chang, T.T., Konzak, C.F., (1974). A decimal code for the growth stages of cereals, 14, 6, 415-421.

Zhang, Y., Hao, Z., Feng, S., Zhang, X., Hao, F., 2022. Changes and driving factors of compound agricultural droughts and hot events in eastern China. Agric. Water Manag. 263, 107485.
Zheng, B., Chenu, K., Fernanda Dreccer, M., Chapman, S.C., 2012. Breeding for the future: what are the potential impacts of future frost and heat events on sowing and flowering time requirements for Australian bread wheat (Triticum aestivium) varieties? Glob. Change Biol. 18, 2899–2914.
Zheng, B., Chapman, S.C., Christopher, J.T., Frederiks, T.M., Chenu, K., 2015. Frost trends and their estimated impact on yield in the Australian wheatbelt. J. Exp. Bot. 66, 3611–3623.
Zhou, S., Zhang, Y., Park Williams, A., Gentine, P.J.Sa, 2019. Projected increases in intensity, frequency, and terrestrial carbon costs of compound drought and aridity events. Sci. Adv. 5, eaau5740.